Approved for public release; distribution is unlimited.

Active Damping Control of a Flexible Space Structure using Piezoelectric Sensors and Actuators

by

Scott M. Newman
Lieutenant, United States Navy
B.S. Aerospace Engineering, United States Naval Academy, 1984

Submitted in partial fulfillment
of the requirements for the degree of

MASTER OF SCIENCE IN ASTRONAUTICAL ENGINEERING

from the

REPORT DOCUMENTATION PAGE

1a. REPORT SECURITY CLASSIFICATION Unclassified		1b. RESTRICTIVE MARKINGS
2a. SECURITY CLASSIFICATION AUTHORITY		3. DISTRIBUTION/AVAILABILITY OF REPORT Approved for public release; distribution is unlimited.
2b. DECLASSIFICATION/DOWNGRADING SCHEDULE		
4. PERFORMING ORGANIZATION REPORT NUMBER(S)		5. MONITORING ORGANIZATION REPORT NUMBER(S)
6a. NAME OF PERFORMING ORGANIZATION Naval Postgraduate School	6b. OFFICE SYMBOL *(If applicable)* 55	7a. NAME OF MONITORING ORGANIZATION Naval Postgraduate School
6c. ADDRESS (*City, State, and ZIP Code*) Monterey, CA 93943-5000		7b. ADDRESS (*City, State, and ZIP Code*) Monterey, CA 93943-5000
8a. NAME OF FUNDING/SPONSORING ORGANIZATION	8b. OFFICE SYMBOL *(If applicable)*	9. PROCUREMENT INSTRUMENT IDENTIFICATION NUMBER
8c. ADDRESS (*City, State, and ZIP Code*)		10. SOURCE OF FUNDING NUMBERS Program Element No / Project No / Task No / Work Unit Accession Number

11. TITLE (*Include Security Classification*)
Active Damping Control of a Flexible Space Structure Using Piezoelectric Sensors and Actuators

12. PERSONAL AUTHOR(S) Newman, Scott M.

13a. TYPE OF REPORT	13b. TIME COVERED	14. DATE OF REPORT (*year, month, day*)	15. PAGE COUNT
Master's Thesis	From To	December 1992	74

16. SUPPLEMENTARY NOTATION
The views expressed in this thesis are those of the author and do not reflect the official policy or position of the Department of Defense or the U.S. Government.

17. COSATI CODES			18. SUBJECT TERMS (*continue on reverse if necessary and identify by block number*)
FIELD	GROUP	SUBGROUP	Active Damping Control, Piezoelectric Sensors and Actuators, Positive Position Feedback, Strain Rate Feedback, Flexible Spacecraft Simulator (FSS)

19. ABSTRACT (*continue on reverse if necessary and identify by block number*)

This thesis details the experimental analysis of an active damping control technique applied to the Naval Postgraduate School's Flexible Spacecraft Simulator using piezoceramic sensors and actuators. The mass property of the flexible arm is varied to study the frequency effects on the Positive Position Feedback (PPF) algorithm. Multi-modal dynamic response is analytically studied using a finite-element model of a cantilevered beam while under the influence of three different control laws: a basic law derived from the Lyapunov Stability Theorem, PPF and Strain Rate Feedback (SRF). The advantages and disadvantages of using PPF and SRF for active damping control are discussed.

20. DISTRIBUTION/AVAILABILITY OF ABSTRACT ☒ UNCLASSIFIED/UNLIMITED ☐ SAME AS REPORT ☐ DTIC USERS	21. ABSTRACT SECURITY CLASSIFICATION Unclassified	
22a. NAME OF RESPONSIBLE INDIVIDUAL Agrawal, Brij N.	22b. TELEPHONE (*Include Area code*) (408) 656-3338	22c. OFFICE SYMBOL AA/Ag

DD FORM 1473, 84 MAR 83 APR edition may be used until exhausted
All other editions are obsolete

ABSTRACT

This thesis details the experimental analysis of an active damping control technique applied to the Naval Postgraduate School's Flexible Spacecraft Simulator using piezoceramic sensors and actuators. The mass property of the flexible arm is varied to study the frequency effects on the Positive Position Feedback (PPF) algorithm. Multi-modal dynamic response is analytically studied using a finite-element model of a cantilevered beam while under the influence of three different control laws: a basic law derived from the Lyapunov Stability Theorem, PPF and Strain Rate Feedback (SRF). The advantages and disadvantages of using PPF and SRF for active damping control are discussed.

TABLE OF CONTENTS

ACKNOWLEDGMENT

The author would like to express his gratitude and appreciation to Dr. Hyochoong Bang for the endless hours of his tutoring, insight and encouragement. The progress of this thesis would not have been achieved without his assistance and expertise. An equal amount of thanks goes to Dr. Brij N. Agrawal for providing the resources used with this project and for guiding the experiment. His assistance with defining the focus of the thesis and his encouragement during difficult times were invaluable.

I. INTRODUCTION

A. BACKGROUND

The evolution of spacecraft into larger and more complex structures, such as Space Station Freedom, has greatly expanded the problem of structural dynamics. The need to limit launch costs drives the engineer to a low mass design which results in these large structures being extremely flexible with very low frequency fundamental vibrational modes. These structural characteristics pose some difficult control problems which are the focus of the emerging Control-Structures Interaction (CSI) field.

There are a variety of scenarios, such as slewing and pointing maneuvers, docking with other spacecraft and interactions with environmental forces that will produce unwanted structural vibrations. There may be requirements for sensor or antenna pointing or attitude control which can not be met with only the inherent structural damping in effect. This describes the need to devise techniques which actively control the dynamic response of flexible structures. Any technique, in simplistic terms, is composed of two separate, but interrelated operations. First, the motion of the structure must be accurately measured by some type of sensor. Then, this information

must be fed back via an effective control algorithm to an actuator on the structure that will counteract the vibrations.

When trying to measure the dynamics of a structure, two possible quantities that can be measured are the acceleration of a point or points on the structural member and the strain within the member. However, with the low frequency vibrations characteristic of the structures we are interested in, precise acceleration measurements are difficult. This leaves strain as the quantity best suited for defining low frequency vibrations.

There are a variety of sensors available for this application such as fiber optic sensors, strain gages and piezoelectric ceramics. Fiber optic sensors can be used to make measurements with a variety of methods, but are not yet practical for complexity and technology problems. Strain gages are limited by a relatively low sensitivity and are highly subject to noise. The one type that has received much study and is seeing increased usage is the piezoelectric ceramic. Reference 1 highlights its advantages as having:

- high strain sensitivity
- low noise
- low to moderate temperature sensitivity
- easy implementation

The desired characteristics of a vibration suppression actuator are low mass, infinite bandwidth, electrically powered and an internal force producer [Ref. 2]. A low mass

requirement is necessary so as not to significantly alter the physical characteristics of the structure as well as the overall launch mass. An ideal infinite bandwidth would theoretically allow control of all vibrational modes of the structure. Electric power reduces the complexity and mass inherent in a mechanical system. An actuator that produces internal forces only would greatly simplify the control algorithm for the entire structure.

A number of materials have been developed for this purpose such as piezoelectric ceramic wafers (PZT), electrorestrictive ceramic wafers (PMN), piezoelectric polymer film (PVF2) and shape memory metal (nitinol) wires. PZT and PMN can produce similar strain levels, but PMN is non-linear and very temperature dependent. Although nitinol can produce strains 300 times greater than PZT, it is difficult to incorporate and not practical for most applications. When considering these tradeoffs, PZT becomes the best choice for an actuator. Its suitability is summarized in the following characteristics [Ref.1]:

- high stiffness
- sufficient stress to control vibrations
- good linearity
- temperature insensitivity
- easy to implement
- low power consumption

To further investigate active damping control techniques, this technology has been incorporated into the Naval Postgraduate School's Flexible Spacecraft Simulator (FSS).

B. FOCUS OF THESIS

The effectiveness and utility of using piezoelectric sensors and actuators to control vibrations will be analytically demonstrated via computer simulations. A model will be developed for a simple cantilevered beam using the finite element method. The dynamic response of this system will be analyzed while under the influence of three different control laws:

- a basic Lyapunov stability-derived control law
- Positive Position Feedback (PPF)
- Strain Rate Feedback (SRF)

The Positive Position Feedback algorithm will also be investigated experimentally. This is the particular control law which has been built into the Flexible Spacecraft Simulator. The mass property of the flexible arm can be adjusted to vary the natural frequency of the first vibrational mode. As will be shown, the effect of the piezoelectric actuator on the dynamic response of the beam will change as the natural frequency varies from a particular optimum value. This will highlight the advantages and disadvatages of this technique.

II. THEORETICAL ANALYSIS

A. PIEZOELECTRIC THEORY

Piezoelectric ceramics and crystals derive their utility in vibration control from the ability to convert electrical energy into mechanical energy and vice versa. When a force is applied to the material, the crystalline structure creates a voltage proportional to the force. Likewise, an electric potential applied across the material will alter its shape dimensionally.

Man-made ceramics have an advantage over natural crystals in that they can be customized for each application. These ceramics can be manufactured in almost any size and shape and have their piezoelectric properties oriented in any specified direction. These properties are induced into the material during a process called "poling". While heated to a temperature above its Curie point, an electric field is applied across the material. This has the effect of realigning the crystalline structure such that it is elongated in a direction parallel to the electric field, the "poling" axis, and foreshortened in a direction perpendicular to the "poling" axis. Henceforth, as shown in Figure 1, any applied voltage of the same polarity as the "poling" voltage will elongate the ceramic along the "poling" axis and a voltage of opposite polarity will elongate

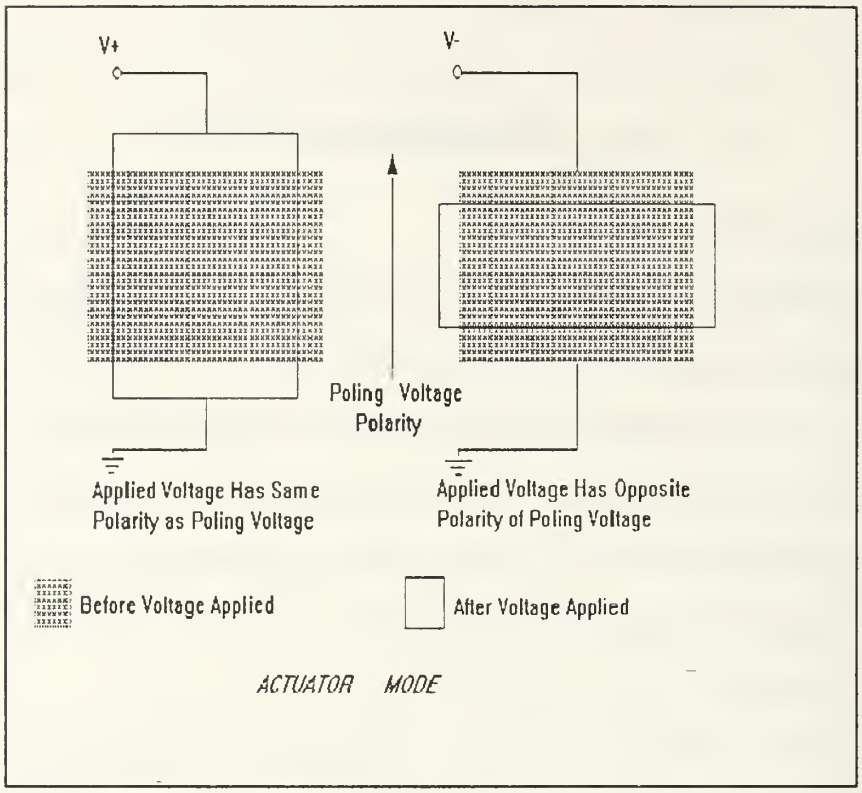

Figure 1 Piezoelectric actuator mode

it in a direction perpendicular to the "poling" axis. In the reverse operation, a parallel compressive force or a perpendicular tensile force in relation to the "poling" axis will produce a voltage of the same polarity and vice versa. (See Figure 2.) [Ref. 3]

The voltage (V_s) produced by a sensor is given by the relationship:

$$V_s = \left(\frac{Ed_{31}}{D}\right) t(e_1 + e_2) \qquad (1)$$

where **E** is the modulus of elasticity of the ceramic, d_{31} is the

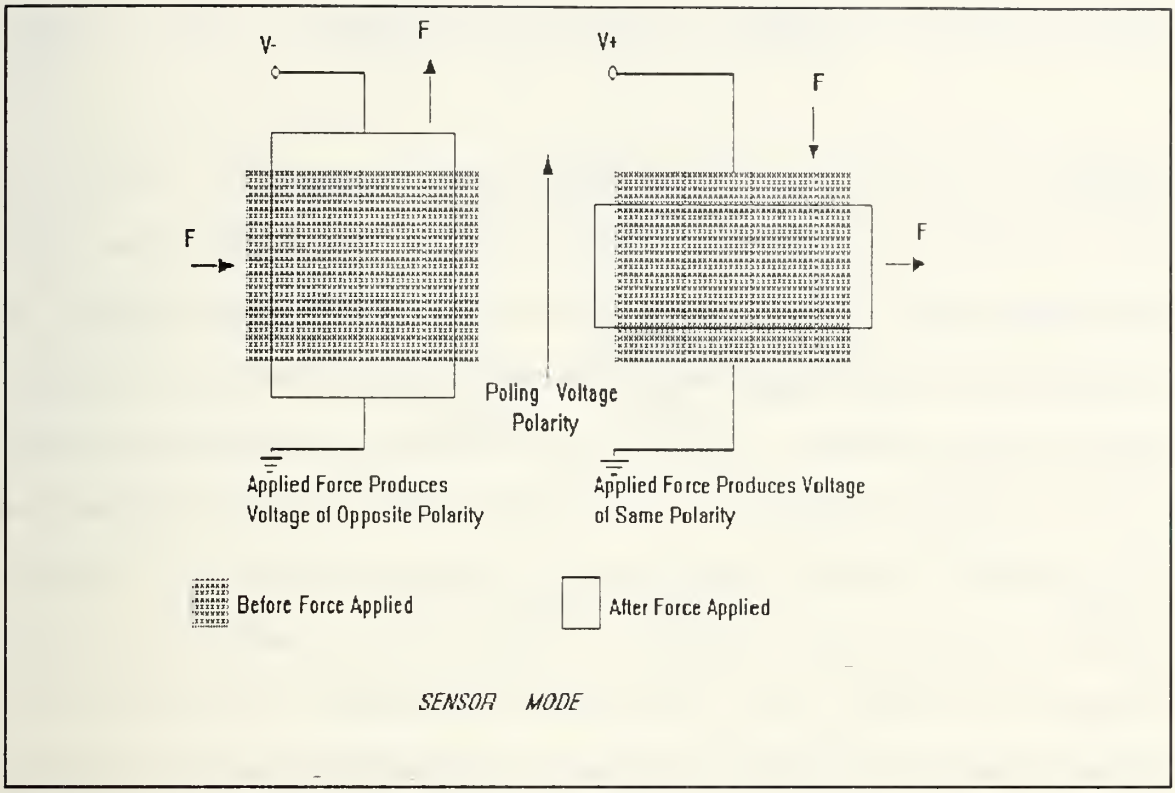

Figure 2 Piezoelectric sensor mode

lateral strain coefficient, **D** is the dielectric constant, **t** is the thickness and ϵ_1 and ϵ_2 are the lateral strains [Ref.4]. This lays the groundwork for measuring the vibration of a structural member by converting the strain on the ceramic produced by the flexural vibrations into a voltage which can be much more easily manipulated and processed.

The effect of an actuator is described by the equation for the bending moment ($\mathbf{m^b(x,t)}$) at a cross-section of the structural member:

$$m^b(x,t) = EIy''(x,t) - k_d v_d(t) \qquad (2)$$

where **EI** is the flexural rigidity of the member, $y''(x,t)$ is the second order partial derivative of the transverse displacement with respect to **x** (the longitudinal coordinate), k_d is a constant dependent on the ceramic piezoelectric constant, dielectric constant, width and the member thickness and $v_d(t)$ is the voltage applied to the ceramic [Ref. 5]. This shows how an applied voltage can produce a strain which, in effect, places concentrated moments (a couple) at the endpoints of the element on which the piezoceramic material is located. The direction of the moment needed to counteract a vibration is changed by changing the polarity of the applied voltage.

B. FINITE ELEMENT MODEL

In order to effectively analyze the dynamic response of a system and the effect of an applied control law, an accurate and workable model of the system must be developed. The finite element method is used to discretize the equations of motion from unwieldy partial differential equations into second-order differential equations of generalized coordinates.

1. Equations of Motion

This analysis will consider a cantilevered beam as the system. From Bernoulli-Euler beam theory, the kinetic energy (**T**), potential energy (**U**), and work (**W**) done by an applied

moment from a piezoceramic actuator (**M(x)**) on each element are:

$$T = \frac{1}{2}\int_{x_1}^{x_1+h} \rho V_e^2 \, dx \tag{3}$$

$$U = \frac{1}{2}\int_{x_1}^{x_1+h} EI \left(\frac{\partial^2 y}{\partial x^2}\right)^2 dx \tag{4}$$

$$W = \int_{x_1}^{x_1+h} M(x) \, \frac{\partial^2 y}{\partial x^2} \, dx \tag{5}$$

where **x** is the coordinate in the longitudinal direction, **y** is the coordinate in the transverse direction, V_e is the transverse velocity, **E** is the modulus of elasticity, **I** is the moment of inertia about the bending axis, ρ is the mass per unit length, x_i is the coordinate of the left end of the element and **h** is the length of the element. A typical finite element is shown in Figure 3 with the associated moment (**M**) and shear (**V**) forces.

From the Extended Hamilton's Principle, the following relationship is used to formulate the equations of motion:

$$\int_{t_1}^{t_2} \delta \, (T-U+W) \, dt = 0 \tag{6}$$

Taking a variation of each term and assuming a constant moment

over the length of the element yields:

$$\int_{t_1}^{t_2}\left[\int_{x_i}^{x_i+h}\rho\dot{y}(\delta\dot{y})\;-\;EI\frac{\partial^2 y}{\partial x^2}\left(\delta\frac{\partial^2 y}{\partial x^2}\right)dx+M\int_{x_i}^{x_i+h}\left(\delta\frac{\partial^2 y}{\partial x^2}\right)dx\right]dt=0 \tag{7}$$

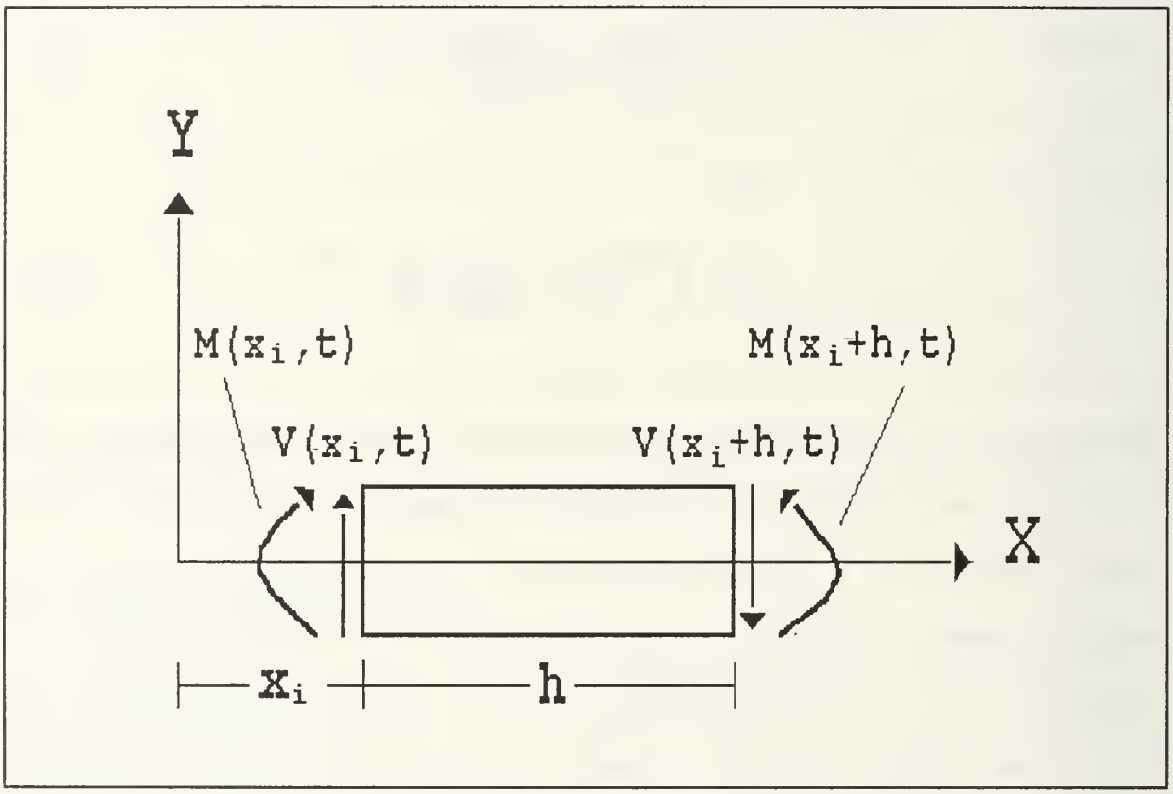

Figure 3 Finite Element Schematic

Integrating the first term by parts gives the following variational equation:

$$\int_{t_1}^{t_2}\left[\int_{x_i}^{x_i+h}-\rho\ddot{y}\delta y\;-\;EI\frac{\partial^2 y}{\partial x^2}\left(\delta\frac{\partial^2 y}{\partial x^2}\right)dx+M\int_{x_i}^{x_i+h}\delta\frac{\partial^2 y}{\partial x^2}\,dx\right]dt=0 \tag{8}$$

At this point, substitutions are made to discretize the motion into the form:

$$y(x,t) = \sum_{i=1}^{4} N_i(x)\ q_i(t) \tag{9}$$

The N_i terms are third-order polynomials, chosen to satisfy the boundary conditions at both ends of the element, which define the mode shapes and are functions of x only [Ref. 6]:

$$\begin{aligned}
N_1 &= 1 - 3\left(\frac{x - x_1}{h}\right)^2 + 2\left(\frac{x - x_1}{h}\right)^3 \\
N_2 &= (x - x_1) - 2h\left(\frac{x - x_1}{h}\right)^2 + h\left(\frac{x - x_1}{h}\right)^3 \\
N_3 &= 3\left(\frac{x - x_1}{h}\right)^2 - 2\left(\frac{x - x_1}{h}\right)^3 \\
N_4 &= -h\left(\frac{x - x_1}{h}\right)^2 + h\left(\frac{x - x_1}{h}\right)^3
\end{aligned} \tag{10}$$

The q_i terms are the system generalized coodinates which are functions of time only. The quantities they represent are:

$$\begin{aligned}
q_1 &= \textit{Transverse Deflection at Left End of Element} \\
q_2 &= \textit{Rotation at Left End of Element} \\
q_3 &= \textit{Transverse Deflection at Right End of Element} \\
q_4 &= \textit{Rotation at Right End of Element}
\end{aligned} \tag{11}$$

Taking the appropriate derivatives of Equation (9) and substituting back into Equation (8) and taking a summation of the ith terms yields:

$$\int_{t_1}^{t_2}\left[\int_{x_1}^{x_1+h}\left(\rho N_1(x)\,\ddot{q}_1(t)\,N_j(x)\,\delta q_j(t) + EIN_1''(x)\,q_1(t)\,N_j''(x)\,\delta q_j(t)\right)dx - M\int_{x_1}^{x_1+h} N_j''(x)\,\delta q_j(t)\,dx\right]dt = 0\,,$$

$$()_1()_1 = \sum_{i=1}^{4}()_i()_i \tag{12}$$

Since this relationship must hold true over any time period and for any arbitrary variation δq_j, the integrand must equal zero. Now, the familiar second-order equation of a vibratory system becomes evident in the form:

$$M_{ij}\ddot{q}_i(t) + K_{ij}q_i(t) = MN_j'(x)\Big|_{x_1}^{x_1+h}\,, \quad j = 1\ldots n \tag{13}$$

The mass (M) and stiffness (K) matrices are computed from:

$$M_{ij} = \rho\int_{x_1}^{x_1+h} N_i(x)\,N_j(x)\,dx$$
$$K_{ij} = EI\int_{x_1}^{x_1+h} N_i''(x)\,N_j''(x)\,dx \tag{14}$$

Performing the integrations results in a system of four equations for each element:

$$\frac{\rho h}{420}\begin{bmatrix}156 & 22h & 54 & -13h\\ 22h & 4h^2 & 13h & -3h^2\\ 54 & 13h & 156 & -22h\\ -13h & -3h^2 & -22h & 4h^2\end{bmatrix}\begin{bmatrix}\ddot{q}_1\\ \ddot{q}_2\\ \ddot{q}_3\\ \ddot{q}_4\end{bmatrix} + \frac{EI}{h^3}\begin{bmatrix}12 & 6h & -12 & 6h\\ 6h & 4h^2 & -6h & 2h^2\\ -12 & -6h & 12 & -6h\\ 6h & 2h^2 & -6h & 4h^2\end{bmatrix}\begin{bmatrix}q_1\\ q_2\\ q_3\\ q_4\end{bmatrix} = M\begin{bmatrix}0\\ -1\\ 0\\ 1\end{bmatrix} \tag{15}$$

The complete mass and stiffness matrices for the entire system are obtained from a simple combination of the elemental matrices. Since the q_3 and q_4 coordinates of one element are the same as the q_1 and q_2 coordinates of the next element, the global matrix is formed by overlapping (adding) the upper left 2x2 submatrix of an element with the lower right 2x2 submatrix of the previous element. Therefore, a n-element system has matrices with dimensions of (nx2)+2 by (nx2)+2. However, for a cantilevered beam, the q_1 and q_2 coordinates of the first element are always zero reducing the matrices to nx2 by nx2.

2. Actuator Moment

The control moment produced by an actuator on an element is derived using the Lyapunov Stability Theorem. The total energy of the beam:

$$U = \frac{1}{2} \int_{x_1}^{x_1+h} \left[\rho \left(\frac{\partial y}{\partial t} \right)^2 + EI \left(\frac{\partial^2 y}{\partial x^2} \right)^2 \right] dx \qquad (16)$$

is chosen as the Lyapunov function. This function meets the requirements of being positive definite, continuously differentiable and equal to zero at the equilibrium state. The only remaining condition needed to ensure stability is that the time derivative of **U** must be less than or equal to zero. [Ref. 7]

The time derivative of the energy function is:

$$\dot{U} = \int_{x_1}^{x_1+h} \left[\rho \dot{y} \ddot{y} + EI \frac{\partial^2 y}{\partial x^2} \frac{\partial}{\partial t} \left(\frac{\partial^2 y}{\partial x^2} \right) \right] dx \qquad (17)$$

Integrating this equation using the following relationships for a vibrating beam, bending moment (M) and shear (V):

$$\rho \ddot{y} + EI \frac{\partial^4 y}{\partial x^4} = 0 \qquad (18)$$

$$M = EI \frac{\partial^2 y}{\partial x^2} \qquad (19)$$

$$V = \frac{dM}{dx} = EI \frac{\partial^3 y}{\partial x^3} \qquad (20)$$

while assuming no shear in the beam yields:

$$\dot{U} = M \left(\dot{y}'_{x_1+h} - \dot{y}'_{x_1} \right) \qquad (21)$$

The quantity in parentheses can be measured by a specially designed electric circuit which amplifies the current developed over the sensor. To ensure that the derivative of the Lyapunov function is always less than zero, M must be of the form:

$$M = -k\left(\dot{y}'_{x_1+h} - \dot{y}'_{x_1}\right) \tag{22}$$

M is directly proportional to the applied voltage to the actuator such that **k** is a positive constant resulting in:

$$\dot{U} = -k\left(\dot{y}'_{x_1+h} - \dot{y}'_{x_1}\right)^2 \leq 0 \tag{23}$$

In terms of the generalized coordinates, the moment is expressed as:

$$M = -k\left(\dot{q}_4 - \dot{q}_2\right) \tag{24}$$

The system of equations for an element with an actuator attached now becomes:

$$M_{ij}\ddot{q}_i + K_{ij}q_i = \begin{bmatrix} 0 & 0 & 0 & 0 \\ 0 & -k & 0 & k \\ 0 & 0 & 0 & 0 \\ 0 & k & 0 & -k \end{bmatrix} \begin{bmatrix} \dot{q}_1 \\ \dot{q}_2 \\ \dot{q}_3 \\ \dot{q}_4 \end{bmatrix} \tag{25}$$

3. Modal Coordinate Form

The equations of motion can be decoupled and more easily analyzed by transforming the generalized coordinates into modal coordinates. This transformation is of the form:

$$q = \Phi\xi \tag{26}$$

where Φ is the weighted modal matrix and ξ is a vector of modal coordinates.

First, the eigenvalues and eigenvectors must be calculated from the freely vibrating undamped system:

$$M\ddot{q} + Kq = 0 \tag{27}$$

For a n-dimensional system, there are n eigenvalues (λ_i, i=1...n) and n eigenvectors (ϕ_i, i=1...n) which satisfy the equation:

$$\lambda_i M\phi_i = K\phi_i \tag{28}$$

The eigenvectors, also known as the normal modes, are orthogonal with respect to the mass and stiffness matrices. This property allows the matrices to be diagonalized using the relationships:

$$\begin{aligned} \phi_i^T M\phi_i &= M_i \\ \phi_i^T K\phi_i &= K_i \end{aligned} \tag{29}$$

where the diagonal elements M_i and K_i, (i=1...n), are known as the generalized mass and stiffness elements for each mode.

The weighted modal matrix (Φ) is obtained by dividing the ith column of the modal matrix by the square root of the ith generalized mass:

$$\Phi_{ij} = \frac{\phi_{ij}}{\sqrt{M_i}} \qquad i=1...n \ , \ j=1...n \qquad (30)$$

Substituting the weighted modal matrix into Equation (29) produces the diagonalizations:

$$\begin{aligned} \Phi^T M \Phi &= I \\ \Phi^T K \Phi &= K^* \end{aligned} \qquad (31)$$

where **I** is the identity matrix and the diagonal elements of K^* are the eigenvalues and squares of the modal frequencies.

If the system is assumed to have viscous damping and excited by an arbitrary function **Fu**, the equations of motion take the form:

$$M\ddot{q} + C\dot{q} + Kq = Fu \qquad (32)$$

If the damping matrix is proportional to either **M** or **K**, it is also diagonalized by the weighted modal matrix. Applying the transformation of Equation (26) to Equation (32) and premultiplying by Φ results in n-uncoupled equations of the form:

$$\ddot{\xi} + \begin{bmatrix} \ddots & & \\ & 2\zeta\omega & \\ & & \ddots \end{bmatrix} \dot{\xi} + \begin{bmatrix} \ddots & & \\ & \omega^2 & \\ & & \ddots \end{bmatrix} \xi = \Phi^T Fu \qquad (33)$$

C. COMPUTER SIMULATIONS

To demonstrate the utility and stability of the specified control laws, the finite element model has been programmed using MATLAB. The basic approach is to put the modal equations into a state-space form and use MATLAB's linear simulator function to produce a time response. The code for the PPF simulation is in the Appendix. The code for the other control laws is of a similar form except for the specific control law formulation.

The following values for the physical parameters of the cantilevered beam were selected:

- number of elements: $n = 8$
- element length: $h = .1$ m
- element density: $\rho = .5$ kg/m^3
- product of modulus of elasticity and moment of inertia: $EI = .9$ Nm^2

Using these values, the system mass and stiffness matrices were formulated and used to solve the eigenvalue problem. That solution provided the modal frequencies of the beam. The first three are:

- $\omega_1 = 7.37$ rad/s $= 1.17$ Hz
- $\omega_2 = 46.19$ rad/s $= 7.35$ Hz
- $\omega_3 = 129.42$ rad/s $= 20.6$ Hz

The inherent structural damping was introduced by arbitrarily damping ratios (ζ_i) such that the damping increased from the lowest value for the first mode to the highest value for the

nth mode. In general, the high frequency modes are damped out more quickly then the lower frequency modes due to the inherent natural frequencies.

For all the simulations, the beam was deflected and released from rest such that the first three modes were excited. Simple geometric calculations were performed to determine the required initial values for each of the generalized coordinates. The open-loop response of the vibrating beam is shown in Figure 4.

From this point on, the simulations are customized to the specific control law utilized. The simulation development and results are detailed in the following sections for each of the three chosen control laws.

1. Lyapunov Stability-Derived Control Law

As shown in Chapter II.B.2, the equations of motion for each element are of the form:

$$M_{ij}\ddot{q}_i + K_{ij}q_i = Fk^*\dot{q}_i \qquad (34)$$

where $\mathbf{k}^*$ is a 1 x 4 vector containing the proportionality factor k:

$$k^* = [\,0\ k\ 0\ -k\,] \qquad (35)$$

F is a 4 x 1 vector dependent on actuator placement. If an actuator is located on an element,

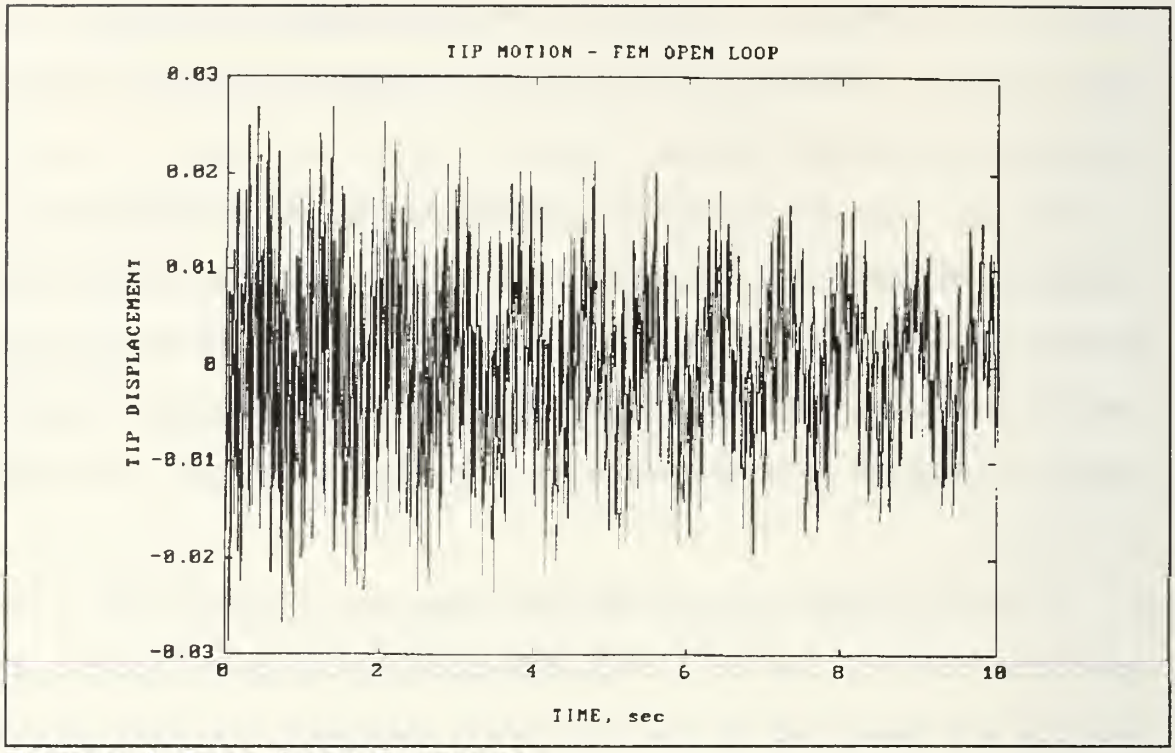

Figure 4 Open-Loop Response

$$F = [\ 0\ -1\ 0\ 1\ ]^T \tag{36}$$

Otherwise, it is a null vector. For the entire system of n elements, the individual 4 x 4 $\mathbf{Fk}^*$ matrices are combined to form the n x n matrix $\mathbf{F}^*$. In modal form, the system is represented by:

$$\ddot{\xi} + (D - \hat{F})\dot{\xi} + K^*\xi = 0 \tag{37}$$

where:

$$D = \begin{bmatrix} 2\zeta_1\omega_1 & & 0 \\ & 2\zeta_2\omega_2 & \\ & & \ddots \\ 0 & & 2\zeta_n\omega_n \end{bmatrix} \qquad \hat{F} = \Phi^T F^* \Phi \qquad K^* = \begin{bmatrix} \omega_1^2 & & 0 \\ & \omega_2^2 & \\ & & \ddots \\ 0 & & \omega_n^2 \end{bmatrix}$$

The system is further manipulated into state space form:

$$\dot{X} = AX + Bu \qquad Y = CX + Du \tag{38}$$

where:

$$X = [\ \xi\ \ \dot{\xi}\ ]^T \qquad A = \begin{bmatrix} 0 & I \\ -K^* & \hat{F} - D \end{bmatrix}$$

C is the identity matrix and B and D are null matrices.

Four different simulations were run with varying actuator locations as follows:

- Case 1. Actuator at base (element 1)
- Case 2. Actuator in middle (element 5)
- Case 3. Actuator at tip (element 8)
- Case 4. Combination of Cases 1-3 (elements 1,5 and 8)

The results are shown in Figures 5-8. As expected, the actuator at the base has the most significant effect on damping vibrations since it can apply the largest moment. Although actuators in the middle and at the tip do provide significant damping when compared to the open-loop response, their contribution is minimal in the combined system. A comparison of Case

1 and Case 4 shows how much the base actuator dominates. This fact highlights the advantage of using a single actuator when considering cost and implementation issues.

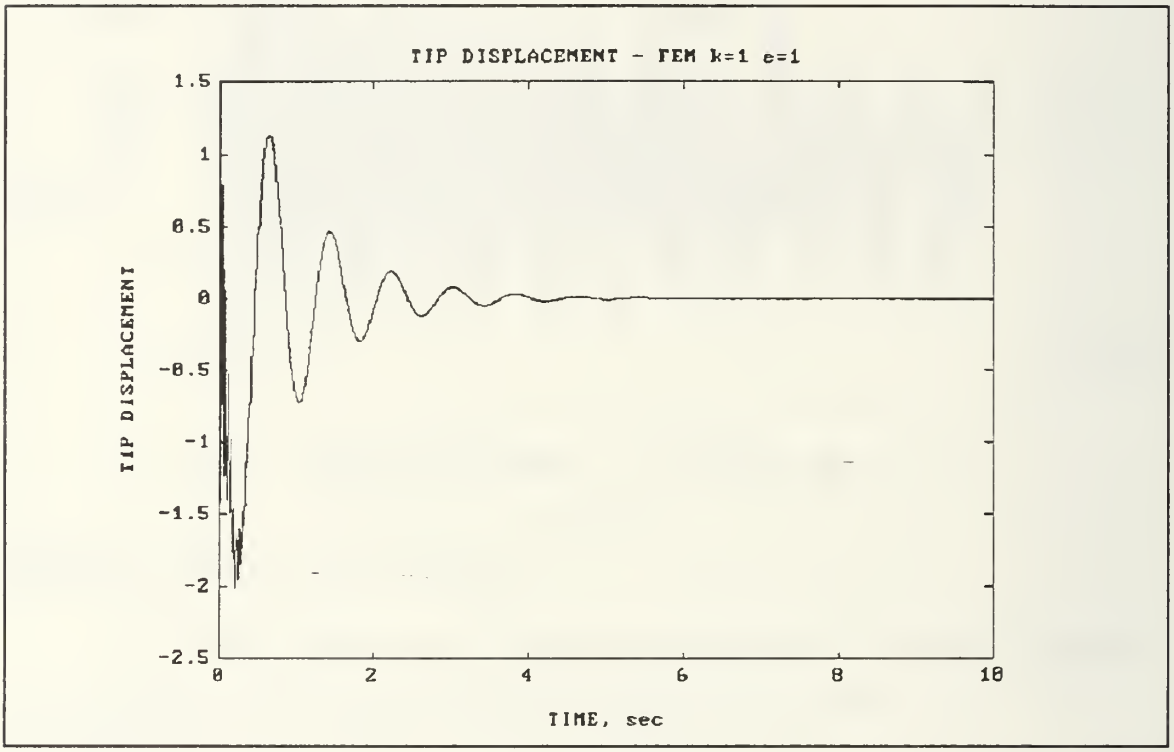

Figure 5 Lyapunov / Actuator at base

The proportionality factor k is a function of the physical constants of the piezoelectric which relate the applied voltage to the moment created and a gain factor applied to the feedback circuit. For simplicity, it is assumed to be unity for these simulations.

Varying **k** has a significant effect on the response. Theoretically, the system is stable for any positive value. However, larger values are, in effect, placing a moment with a magnitude larger than required which tends to "overcontrol"

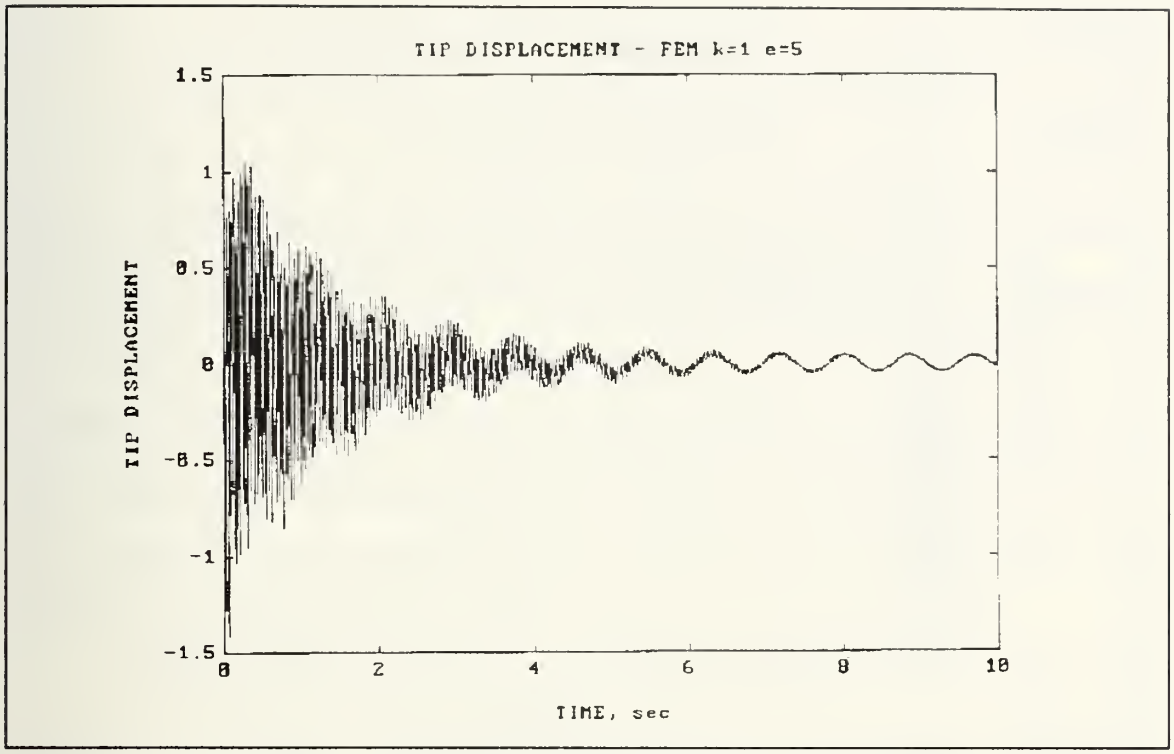

Figure 6 Lyapunov / Actuator in middle

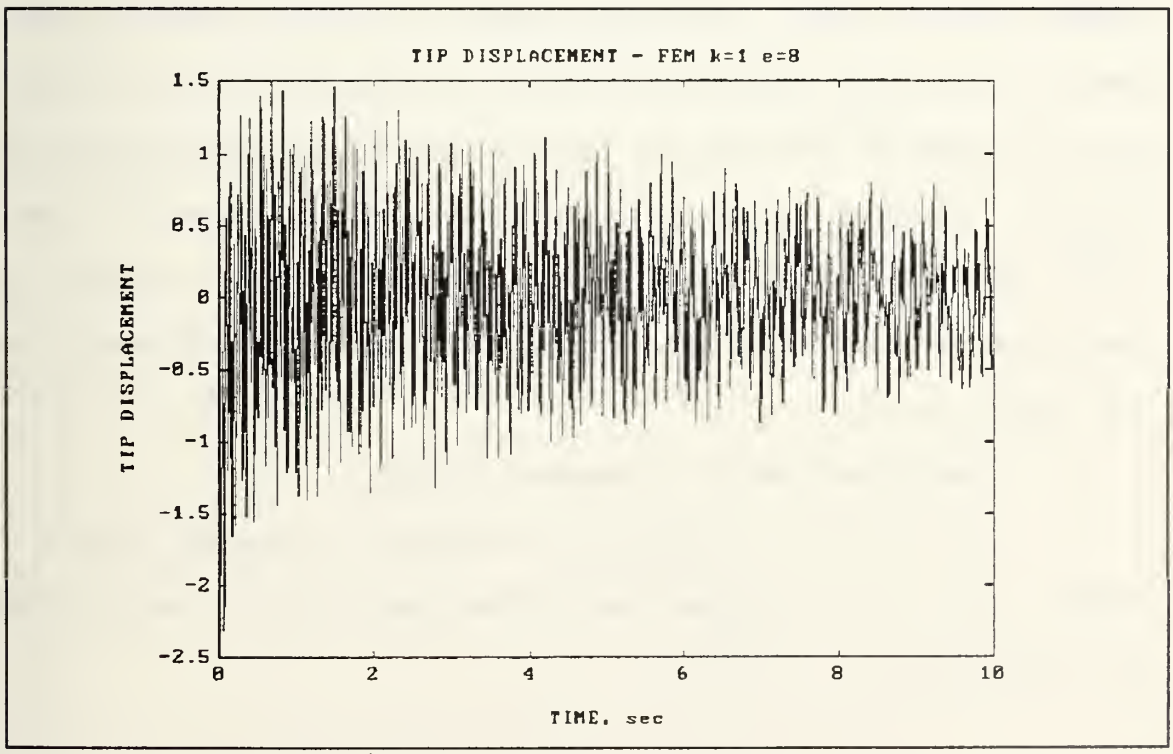

Figure 7 Lyapunov / Actuator at tip

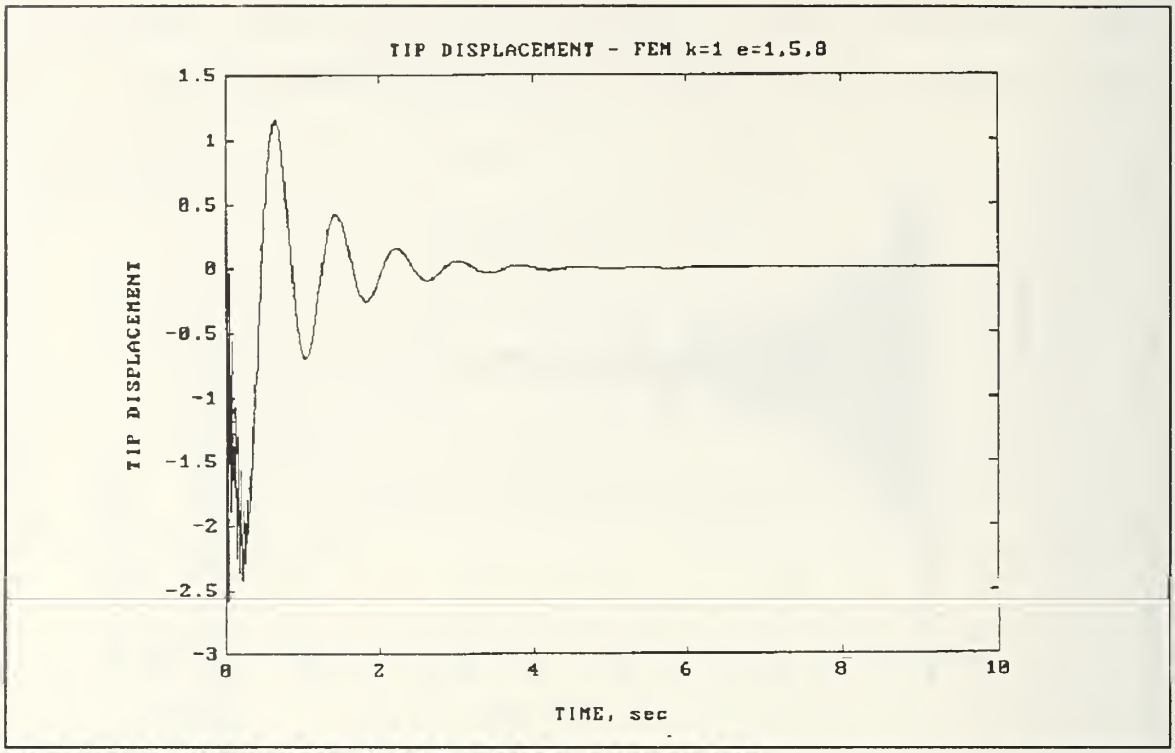

Figure 8 Lyapunov / All three actuators

the beam. This is seen in the response as the actuators, although stabilizing, drive the beam to excessive amplitudes. Small values of **k** equate to moments of insufficient magnitude which decrease the damping ratio. Optimizing the system requires a tradeoff between the desired settling time and a maximum allowable amplitude. A trial and error procedure is required to select the best value and customize the control to the application.

2. Positive Position Feedback (PPF)

This control algorithm is defined strictly in the modal form. For a scalar case, the equations of motion are represented by:

$$\ddot{\xi} + 2\zeta\omega\dot{\xi} + \omega^2\xi = G\omega^2\eta \tag{39a}$$

$$\ddot{\eta} + 2\zeta_c\omega_c\dot{\eta} + \omega_c^2\eta = \omega_c^2\xi \tag{39b}$$

where ξ is the structure modal coordinate, η is the compensator modal coordinate, ζ and ζ_c are the structure and compensator damping ratios, ω and ω_c are the structure and compensator natural frequencies and G is a gain factor. As seen in Equation (39), PPF means positively feeding the structure coordinate back to the compensator and positively feeding back the compensator coordinate times a gain to the structure.

The system response characteristics of this algorithm are shown in Figure 9. Assuming that the structure motion at steady state is of the form:

$$\xi(t) = \alpha e^{i\omega t} \tag{40}$$

the compensator will respond as:

$$\eta(t) = \beta e^{i(\omega t - \phi)} \tag{41}$$

where the phase angle, ϕ, is defined by:

$$\phi = \tan^{-1}\left(\frac{2\zeta_c\frac{\omega}{\omega_c}}{1 - \left(\frac{\omega}{\omega_c}\right)^2}\right) \tag{42}$$

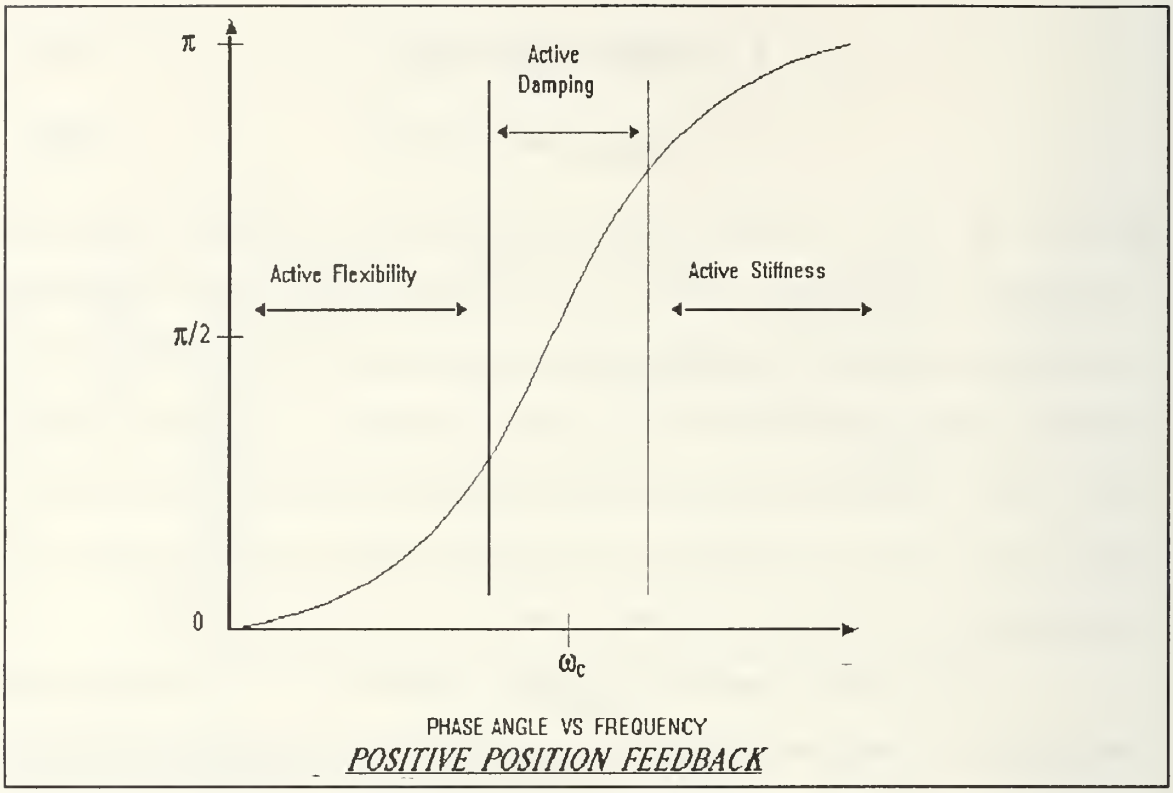

Figure 9 Positive Position Feedback

When the structure vibrates at a frequency much lower than the compensator natural frequency, the phase angle approaches zero. Substituting Equation (41) with $\phi = 0$ back into Equation (39a) gives:

$$\ddot{\xi} + 2\zeta\omega\dot{\xi} + (\omega^2 - G\beta\omega^2)\xi = 0 \qquad (43)$$

resulting in a decrease in the stiffness term. When the structure and compensator have the same natural frequency, the phase angle is $\pi/2$. In this case, the structural equation is modified to:

$$\ddot{\xi} + (2\zeta\omega + G\beta\omega)\dot{\xi} + \omega^2\xi = 0 \qquad (43)$$

showing an increase in damping. When the structure is vibrating a frequency much greater than the compensator natural frequency, the phase angle approaches π. Making the same substitution yields:

$$\ddot{\xi} + 2\zeta\omega\xi + (\omega^2 + G\beta\omega^2)\xi = 0 \qquad (45)$$

causing an increase in the stiffness term. These equations clearly show that, in order to maximize damping, ω_c must be as closely matched to ω as possible.

This analysis will go beyond the simple scalar case and investigate a multi-modal vibration suppression system. Specifically, the first three modes will be controlled using two different schemes. First, three collocated sensor/actuator pairs connected to three compensators tuned to the first three modal frequencies will be analyzed. The second system will utilize only one collocated sensor/actuator pair connected to the same compensators. Figures 10 and 11 illustrate these two configurations with simple block diagrams.

In a multi-modal case, the system equations take the form:

$$\ddot{\xi} + D\dot{\xi} + K\xi = C^T GK\eta \qquad (46a)$$

$$\ddot{\eta} + D_c\dot{\eta} + K_c\eta = K_c C\xi \qquad (46b)$$

For a system with n structural modes and m compensators, ξ is

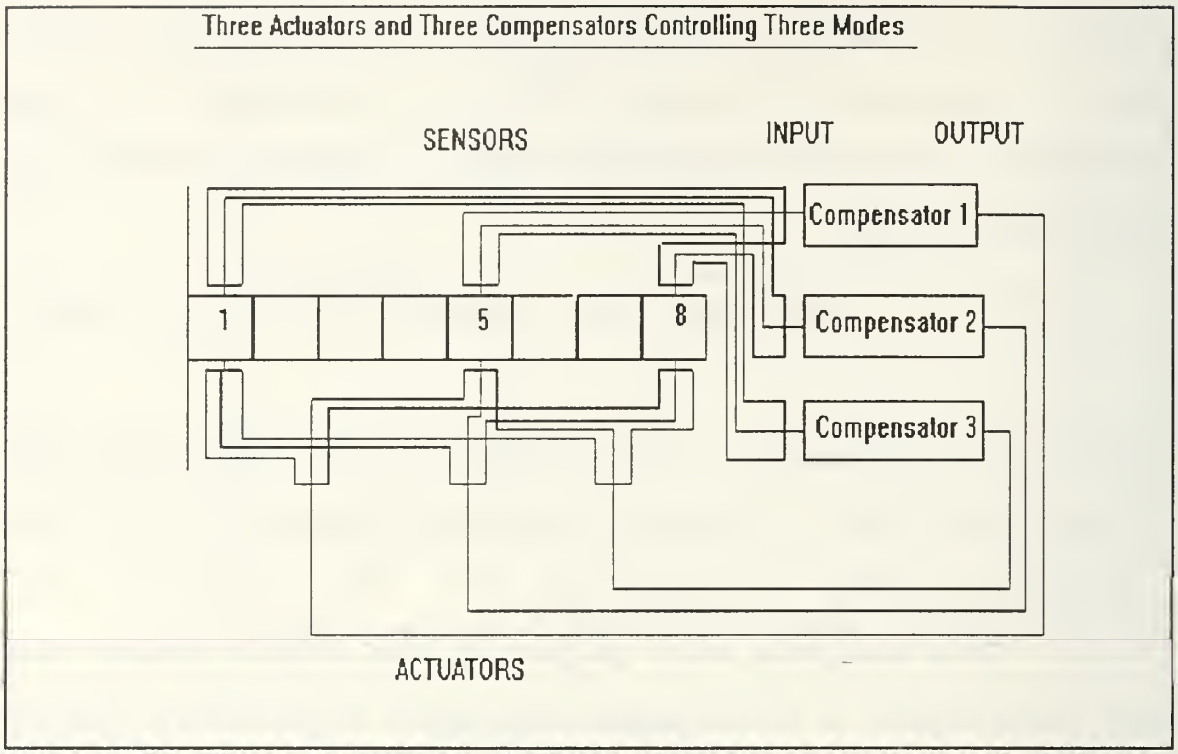

Figure 10 Three Actuator / Three Compensator Control Scheme

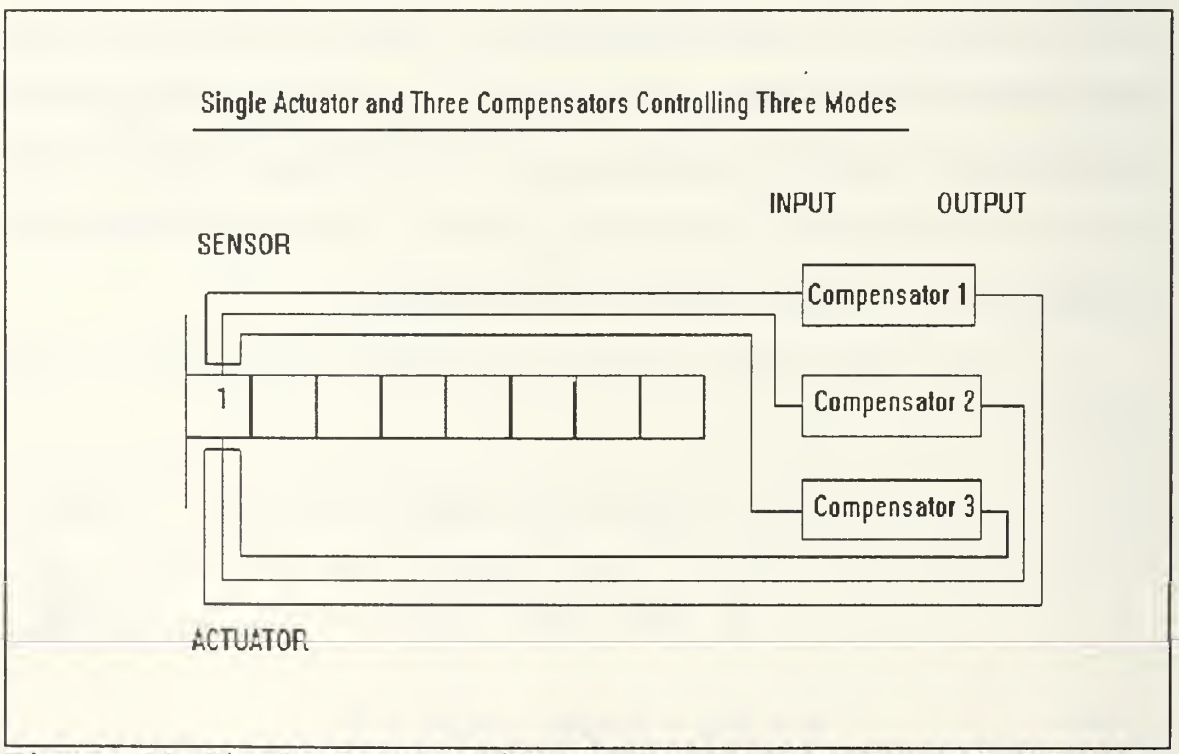

Figure 11 Single Actuator/Three Compensator Control Scheme

a [n x 1] vector and η is a [m x 1] vector. **D** and $\mathbf{D}_c$ are [n x n] and [m x m] diagonal matrices containing the damping terms $2\zeta_i\omega_i$ and $2\zeta_{ci}\omega_{ci}$. **K** and $\mathbf{K}_c$ are [n x n] and [m x m] diagonal matrices containing the squares of the natural frequencies ω^2_i and ω^2_{ci}. **G** is a [m x m] diagonal matrix of compensator gains. **C** is a fully populated [m x n] participation matrix which determines the influence of each sensor/actuator pair on each compensator and vice versa.

The formulation of these matrices is straightforward except for the participation matrix. Equating the right hand sides of Equations (33) and (46a):

$$\Phi^T F u = C^T G K \eta \tag{45}$$

and assuming the control vector **u** is equal to the vector $\mathbf{GK}\eta$, **C** is equal to $(\Phi^T\mathbf{F})^T$. **u** is a [p x 1] vector, where p is the number of actuators, which forces the dimensions of $\Phi^T\mathbf{F}$ to be [n x p]. A modification must be made in the case of the single actuator (u = 1). In order to keep the **G** and **K** matrices in the same form and ensure dimensional compatibility, a [1 x m] vector **A** whose elements are unity must be included such that:

$$\Phi^T F u = C^T A G K \eta \tag{48}$$

Now the entire system can be put into the matrix form:

$$\begin{bmatrix} \ddot{\xi} \\ \ddot{\eta} \end{bmatrix} + \begin{bmatrix} D & 0 \\ 0 & D_c \end{bmatrix} \begin{bmatrix} \dot{\xi} \\ \dot{\eta} \end{bmatrix} + \begin{bmatrix} K & -C^T(A)GK \\ -K_c(A^T)C & K_c \end{bmatrix} \begin{bmatrix} \xi \\ \eta \end{bmatrix} = 0 \qquad (49)$$

As was done in Chapter II.C.1 with Equation (38), a state-space transformation is made to perform the simulations. The same initial conditions are used to excite the tri-modal vibration previously shown in Figure 4. The compensator natural frequencies were chosen to exactly match the structural frequencies in order to maximize the damping effect. In this case, the com-pensator damping ratio, ζ_c, should be as small as possible. As shown in Figure 12, this creates a resonance peak near the compensator frequency allowing the largest gain possible to act on the affected mode in the active damping region. This will also diminish the effects of active flexibility on lower modes. For these simulations, it was assumed that each compensator could be designed to have a damping ratio equal to .1. In actuality, it will be very unlikely that the compensators can be designed as precisely as they have been here and a decrease in system performance is expected. To prevent a significant decrease, the compensator damping ratio should be increased so that the active damping region is widened as much as possible.

Figure 13 shows the response of the beam under the influence of three actuators at the base, in the middle and at

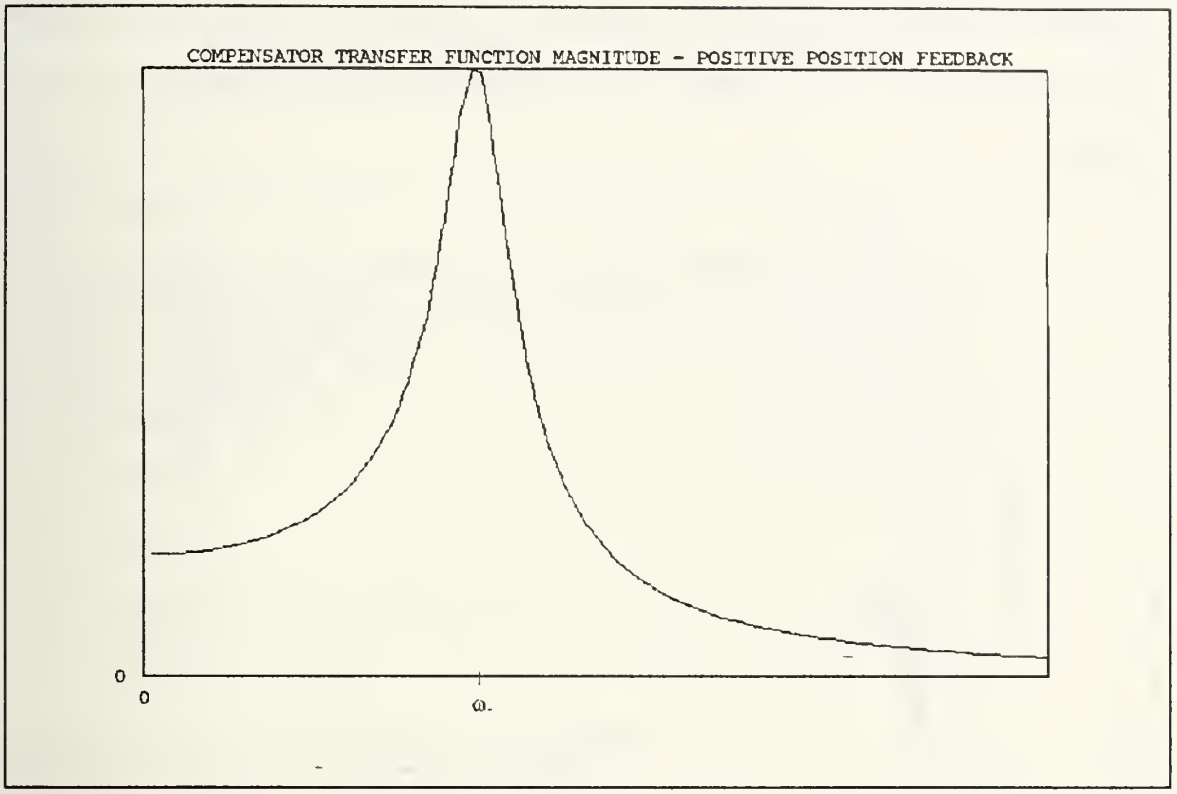

Figure 12 PPF Compensator Transfer Function Magnitude

the tip. The effectiveness of this system is seen in how quickly all three modes are suppressed. A single actuator at the base also provides a sufficient degree of control as seen in Figure 14. The effect of actuator placement is evident in a comparison with Figures 15 and 16 which correspond to a single actuator in the middle and at the tip, respectively, feeding the same compensators with the same gains. However, the performance of these last two configurations can be improved by increasing the gains. Due to the fact that a larger moment can be placed at the tip than at the base without driving the beam unstable, the allowable gains are two orders of magnitude greater for Case 3 than Case 1. The individual modal

responses can also be tailored by varying the gains such that the damping of one mode is maximized in relation to the others.

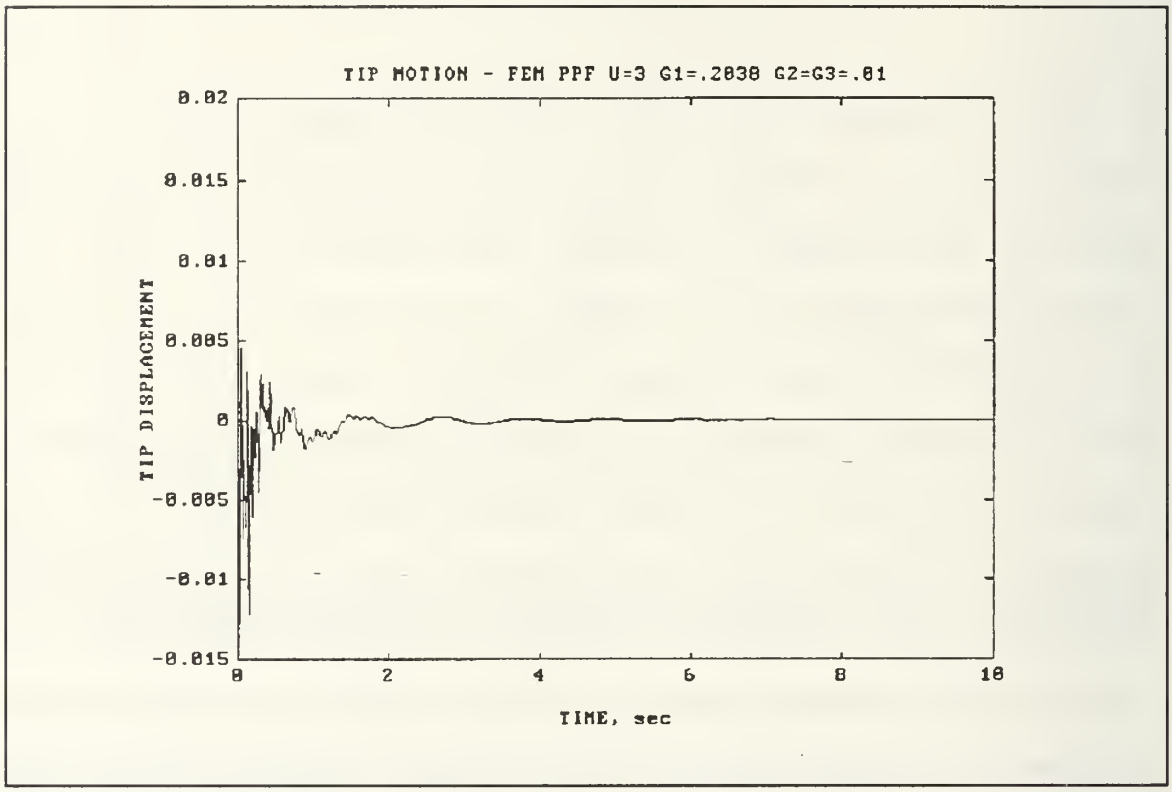

Figure 13 PPF Three Actuators

In the scalar case, system stability is clearly defined. A simple manipulation of the equations of motion and application of the Routh-Hurwitz criterion results in the condition:

$$0 < G < 1 \tag{50}$$

This method is not applicable to the much more complex multimodal case. Fanson and Caughey have developed the following stability condition:

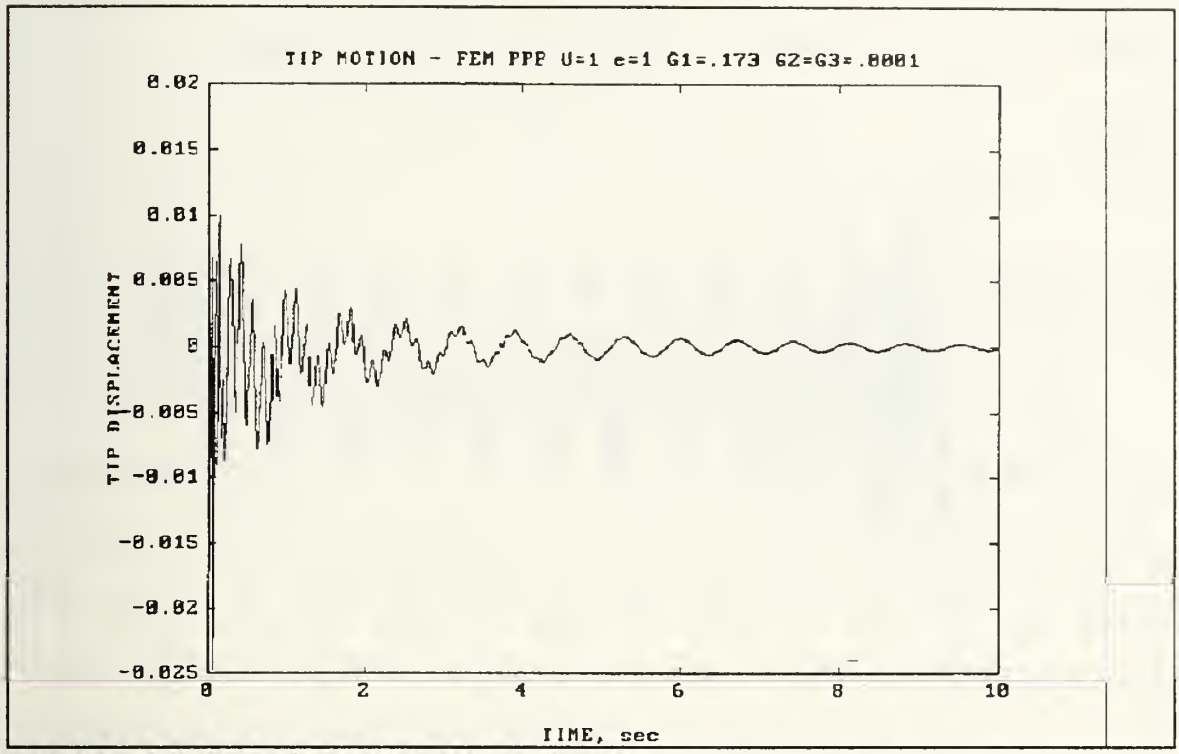

Figure 14 PPF / Actuator at base

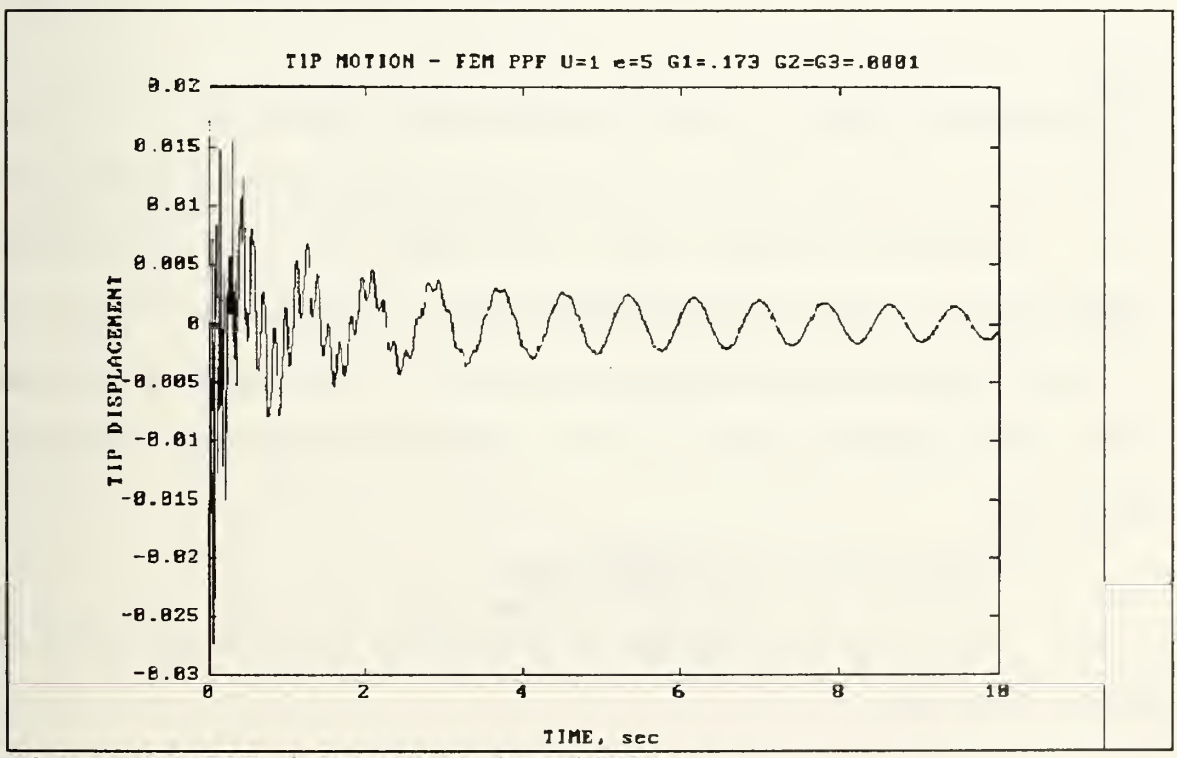

Figure 15 PPF / Actuator in middle

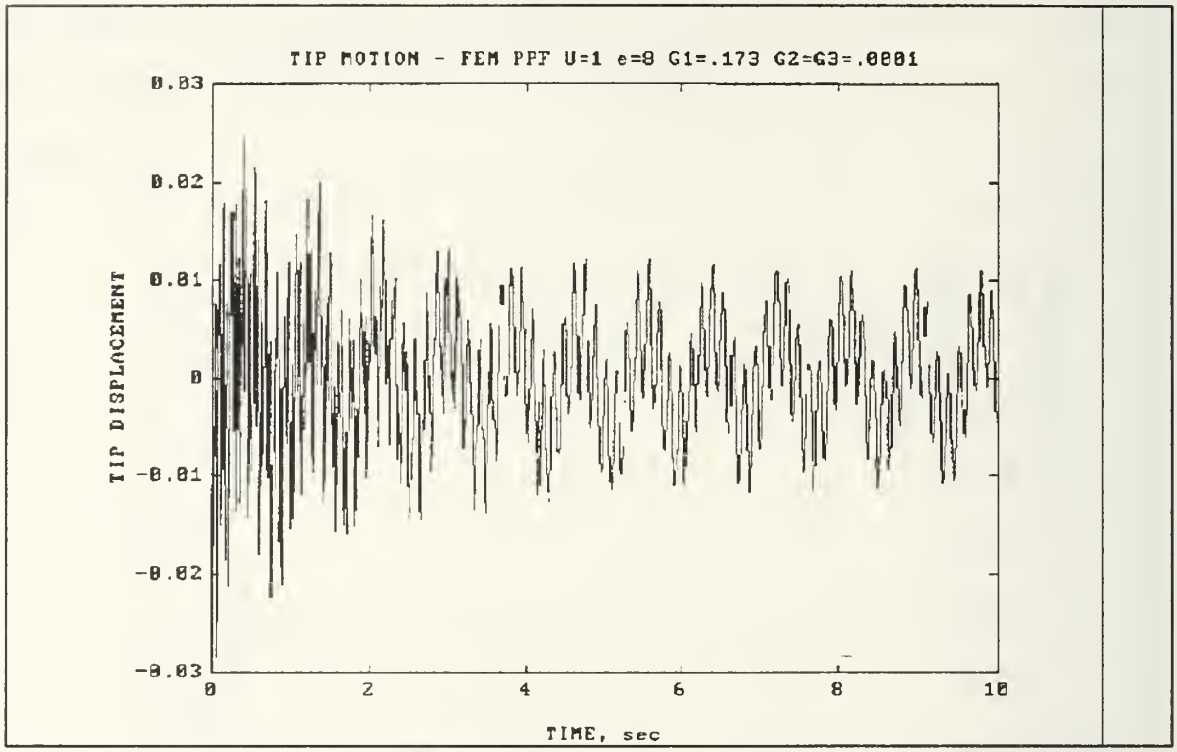

Figure 16 PPF / Actuator at tip

$$K - C^T GKC > 0 \tag{51}$$

for employing PPF in a multi-modal system [Ref. 8]. This condition is limited in that this single criterion is a function of m variables which are the gains of the individual compensators. The procedure used for these simulations was to fix two gains while varying the third to determine the range where the eigenvalues of the assembled matrix were all positive.

3. Strain Rate Feedback (SRF)

The final algorithm investigated is also defined in modal form as:

$$\ddot{\xi} + 2\zeta\omega\dot{\xi} + \omega^2\xi = -G\omega^2\eta \tag{52a}$$

$$\ddot{\eta} + 2\zeta_c\omega_c\dot{\eta} + \omega_c^2\eta = \omega_c\xi \tag{52b}$$

where the variables are the same as those previously defined for PPF. In this case, the structural velocity coordinate is fed back to the compensator and the compensator position coordinate is fed back times a negative gain to the structure. The gain must be negative, as will be shown in the following analysis, so that the system performance will be optimized over the most useful frequency range. Figure 17 graphically summarizes the performance characteristics of SRF.

If we again assume that the structural modal coordinate is of the form:

$$\xi(t) = \alpha e^{i\omega t} \tag{53}$$

the compensator response will be:

$$\eta(t) = \beta e^{i(\omega t - \phi)} \tag{54}$$

where ϕ is now defined by:

$$\phi = \tan^{-1}\left(\frac{\left(\frac{\omega}{\omega_c}\right)^2 - 1}{2\zeta_c\frac{\omega}{\omega_c}}\right) \tag{55}$$

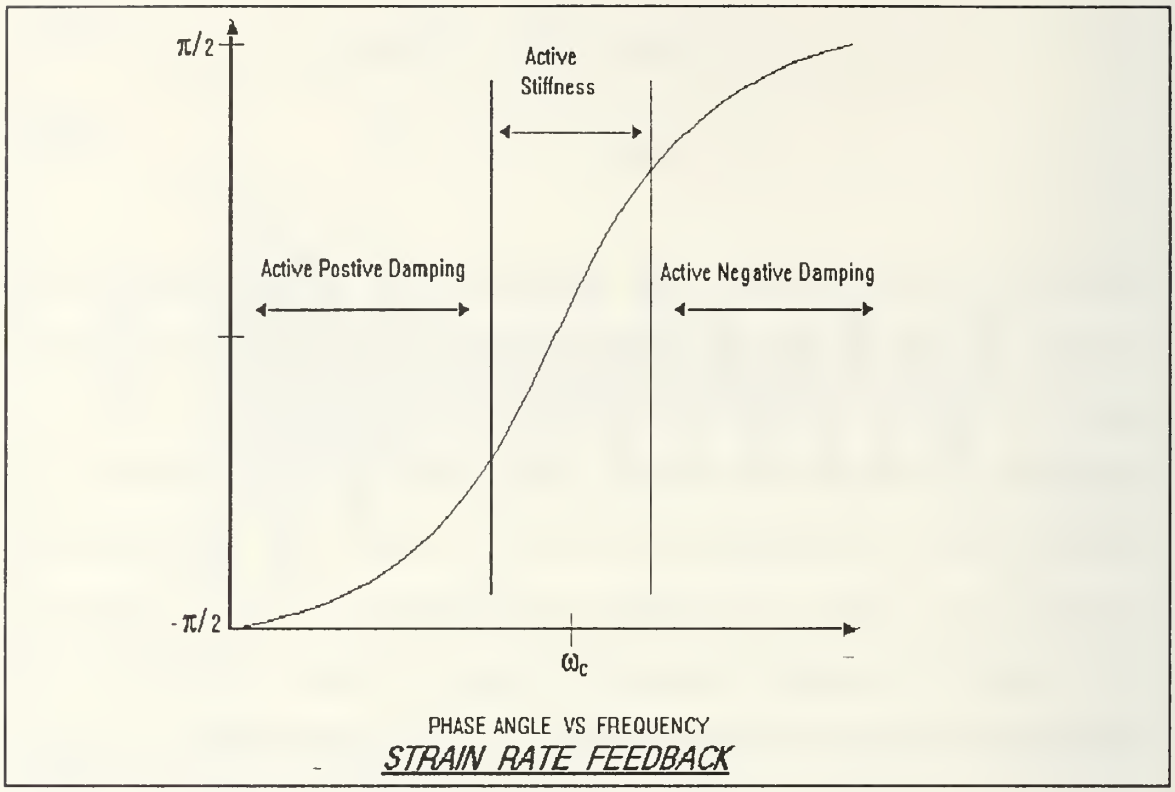

Figure 17 Strain Rate Feedback

When $\omega << \omega_c$, the phase angle, ϕ, approaches $-\pi/2$. Substituting Equation (54) with $\phi = -\pi/2$ back into Equation (52a) gives:

$$\ddot{\xi} + (2\zeta\omega + G\beta\omega)\dot{\xi} + \omega^2\xi = 0 \qquad (56)$$

resulting in an increase in damping. When $\omega = \omega_c$, $\phi = 0$ and a similar substitution yields:

$$\ddot{\xi} + 2\zeta\omega\dot{\xi} + (\omega^2 + G\beta\omega^2)\xi = 0 \qquad (57)$$

increasing the stiffness of the structure. Finally, when $\omega >> \omega_c$, $\phi = \pi/2$ and the structure response is:

$$\ddot{\xi} + (2\zeta\omega - G\beta\omega)\dot{\xi} + \omega^2\xi = 0 \qquad (57)$$

showing a decrease in damping. The obvious conclusion is to design the compensator such that the structural frequencies of the modes to be damped fall well below the compensator natural frequency.

The SRF simulations were done using the same format as the PPF simulations. The first three structural modes were controlled using three compensators and the same four sensor/actuator configurations. Additionally, the possibility of controlling the first three modes using only one compensator and one actuator is investigated. The participation matrix formulation is identical to the PPF case. The state-space transformation is applied to the system defined by:

$$\begin{bmatrix} \ddot{\xi} \\ \ddot{\eta} \end{bmatrix} + \begin{bmatrix} D & 0 \\ -\omega_c(A^T)C & D_c \end{bmatrix} \begin{bmatrix} \dot{\xi} \\ \dot{\eta} \end{bmatrix} + \begin{bmatrix} K & C^T(A)GK \\ 0 & K_c \end{bmatrix} \begin{bmatrix} \xi \\ \eta \end{bmatrix} = 0 \qquad (59)$$

Selecting a precise compensator frequency is not as clearly defined as it is with PPF. Additionally, the stability condition is not as clearly as defined as in the PPF case due to the fact that the closed-loop damping and stiffness matrices can not be symmetrized. However, the wider active damping region gives the designer a lot more flexibility in the circuit design. As long as the compensator frequency is greater than the structural frequency, a certain amount of active

damping will be provided. Although the stabilizing feedback gain matrix is heavily dependent upon the structure and compensator frequencies, some numerical analyses predict that higher compensator frequencies produce larger damping ratios. A drawback to frequencies in this range is that, as shown in Figure 18, the magnitude of the compensator transfer function approaches zero limiting the amount of control. Further study is required on this point. Again, the compensators were assumed to have damping ratios equal to .1. To highlight the effects of varying compensator frequencies, simulations were run for the three actuator/three compensator configuration with two different sets of ω_c at the two extremes. First, the compensators were assigned frequencies ten per cent higher than each of the structural modes. This response is seen in Figure 19. Although the higher modes are controlled, the first mode is not significantly damped. The system is operating too far in the active stiffness region. The dominance of the active stiffness can be seen in the higher frequency of the first mode. The second set of compensator frequencies were 50 times higher than each of the structural modes. This has the effect of placing all three structural modes in the active damping region of all three compensators. This response is shown in Figure 20. In this case, the transfer function magnitudes are so small that gains four orders of magnitude larger than the previous case are needed. With these large gains, the higher

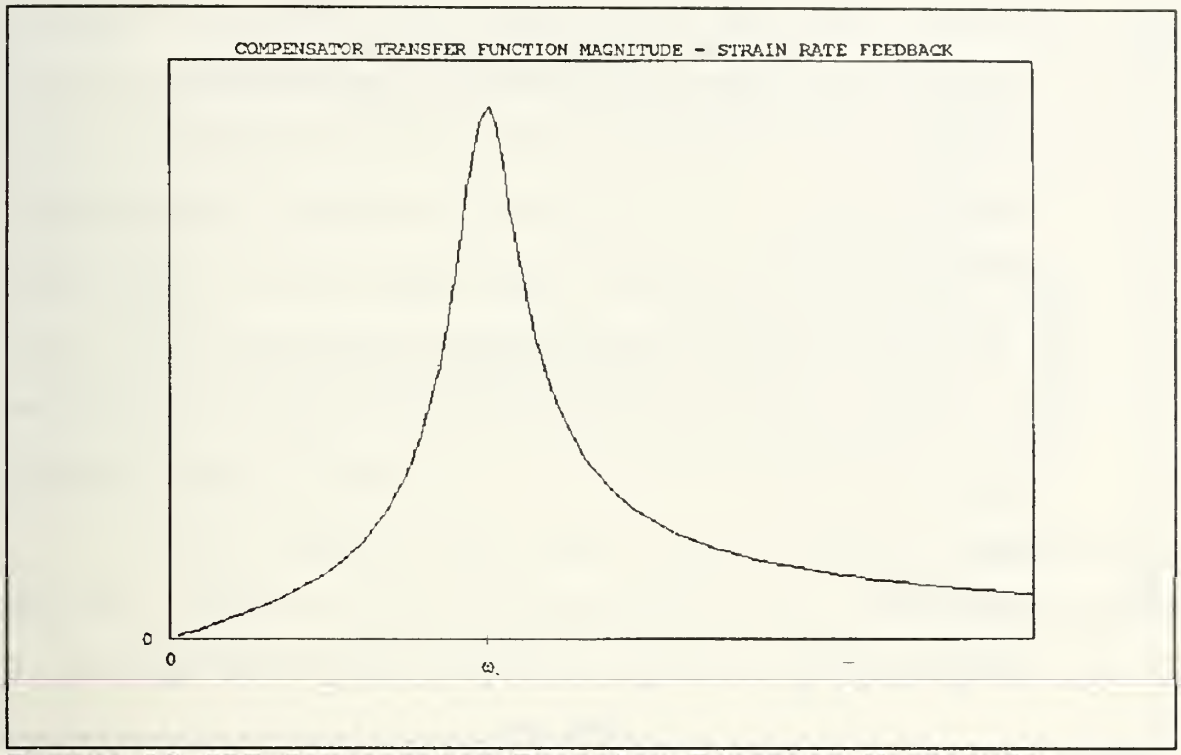

Figure 18 SRF Compensator Transfer Function Magnitude

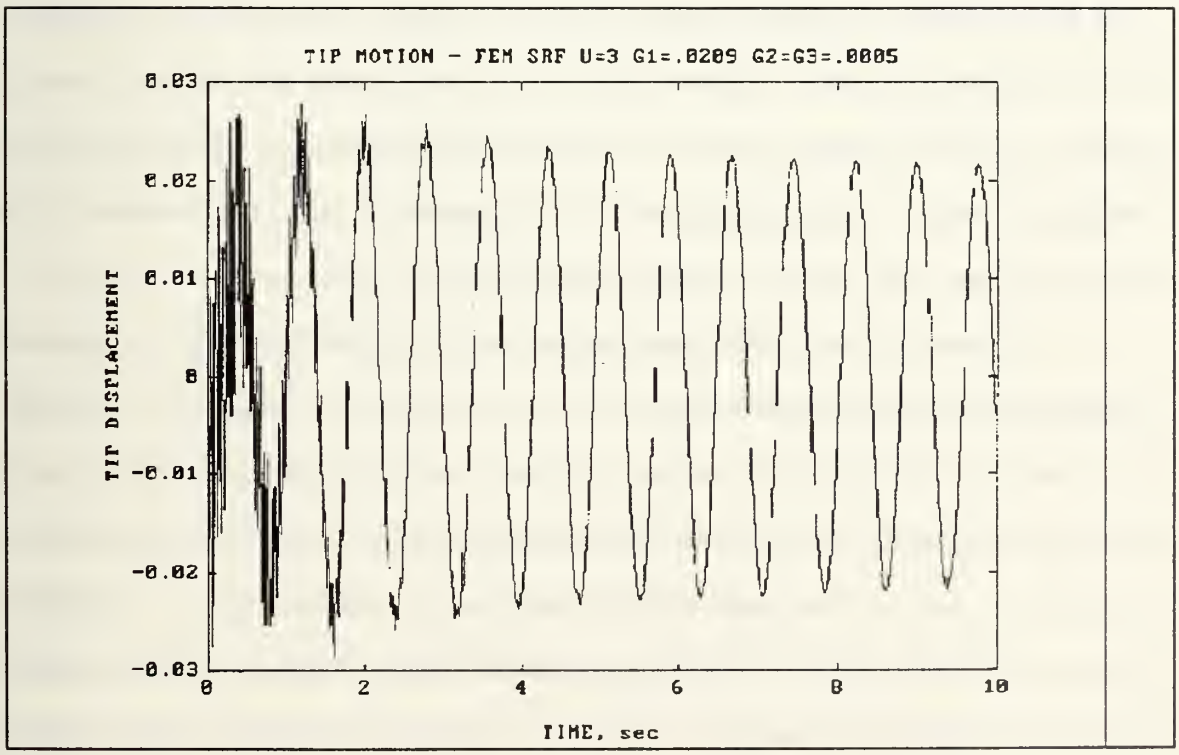

Figure 19 SRF ω_c = 1.1 x ω

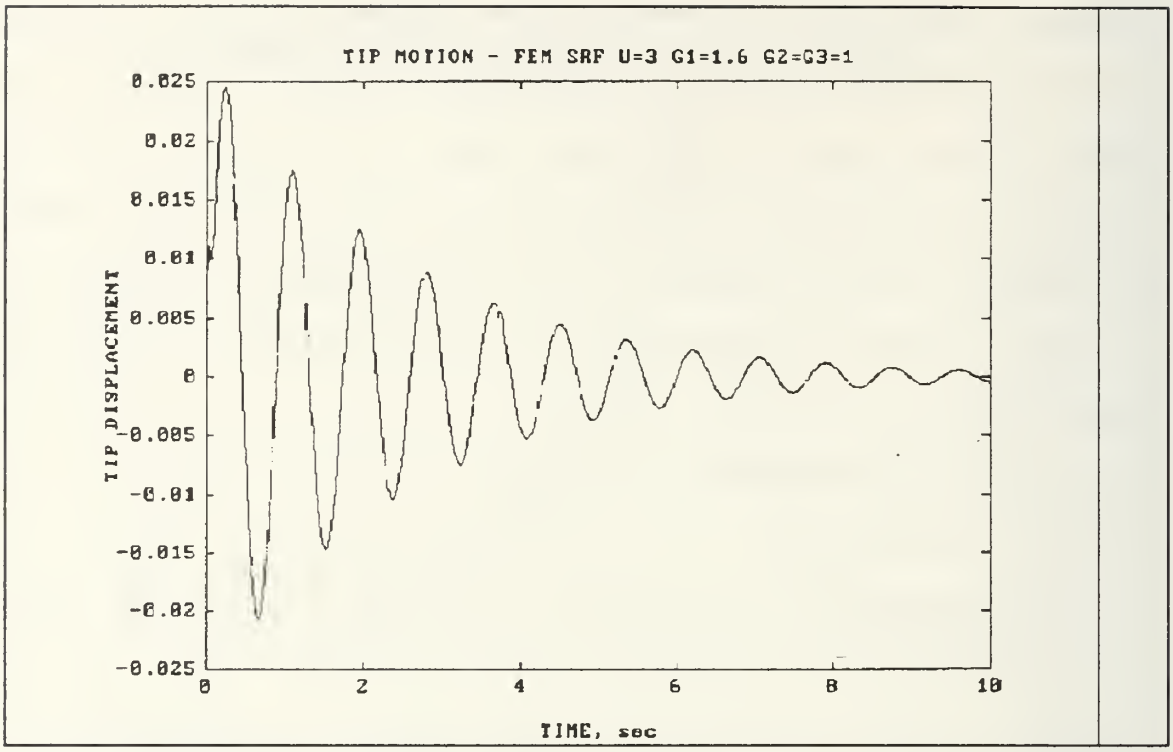

Figure 20 SRF $\omega_c = 50 \times \omega$

modes are almost immediately suppressed. The first mode, having the lowest relative gain, is not controlled as efficiently. A significant improvement in performance occurs as ω_c moves farther away from ω. The same variation in the system response when the single actuator moves from the base to the tip is seen as in the PPF simulations.

The control system can be simplified by only using one compensator and one actuator at the base as shown in Figure 21. The motivation for this approach comes from the results of the three compensator case where all three structural frequencies were below the smallest compensator frequency. Theoretically, a compensator will provide active damping to all modes with a lesser frequency. For this simulation, the compensator

frequency was set at ten times the third modal frequency. The system matrices must be modified because the compensator equation is now in a scalar form. As shown in Figure 22, this configuration effectively controls all three modes with maximum effect on the higher modes. However, this method will only work for a few densely spaced modes. If the frequency range is expanded too far, the lower modes will not receive a strong enough control input.

This approach was also taken using an alternative method. The sign of the gain applied to the compensator ouput is changed such that the structural modal equation is now:

$$\ddot{\xi} + 2\zeta\omega\dot{\xi} + \omega^2\xi = G\omega^2\eta \qquad (60)$$

This has the effect of swapping the regions of active positive damping and active negative damping and making the region centered around ω_c active flexibility. Now, the objective is to set the compensator frequency below the first mode placing all the modes in the active positive damping region. In this simulation, the compensator frequency was set at 80% of the first modal frequency. A first attempt was made using the same compensator damping ratio ($\zeta_c = .1$). This was an unstable system due to the resonance peak of the compensator transfer function occuring in the active flexibility region. To improve the response, the damping ratio of the compensator had to be increased such that there was no resonance and the flexibility effect was diminished with respect to the damping effect. A

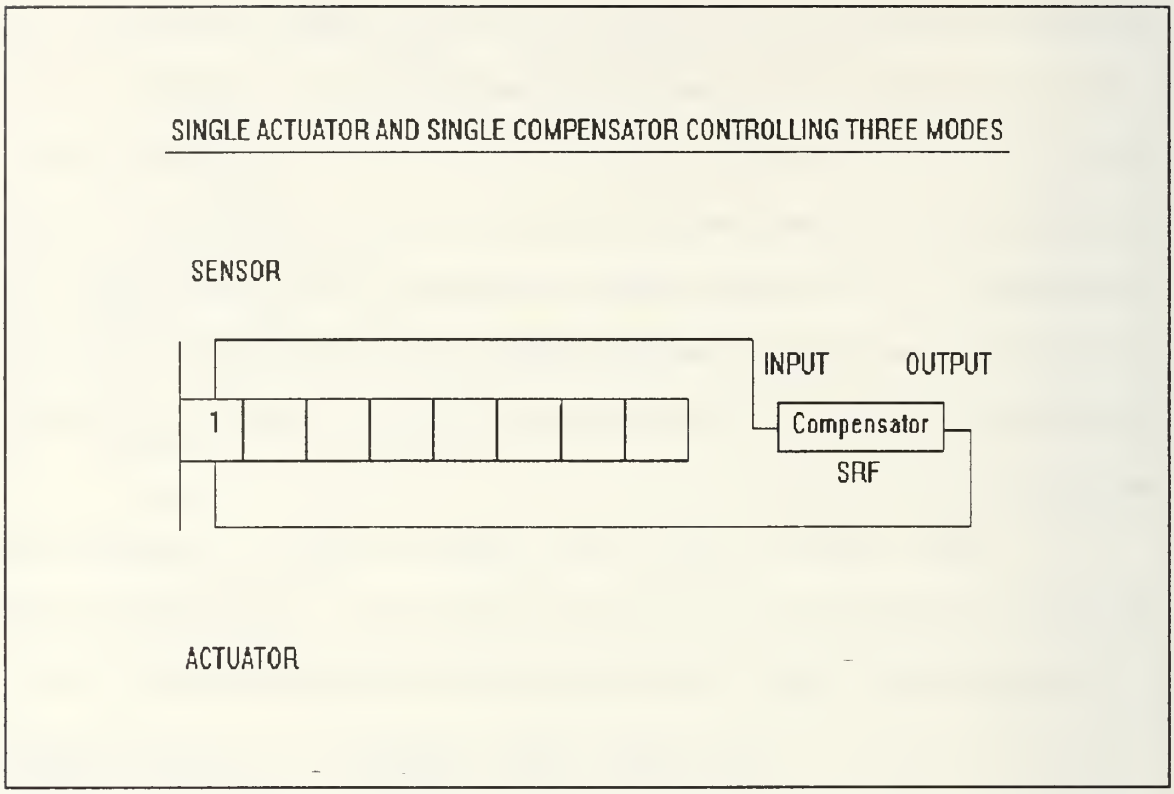

Figure 21 Single Actuator/Single Compensator Control Scheme

value for ζ_c of .95 produced the response in Figure 23. As expected, the higher modes are not damped out as quickly as in the previous case. To prevent the first mode from being driven unstable, the gain must be held relatively low which reduces the impact at higher frequencies. In practice, the effective bandwidth of the actual compensator must be considered. The compensator will damp only those modes densely packed within the range of control.

Deriving a stability condition for SRF similar to Equation (51) for PPF proved difficult. A transformation to symmetrize the modal equations could not be found. In their unsymmetric form, the equations could not be manipulated to

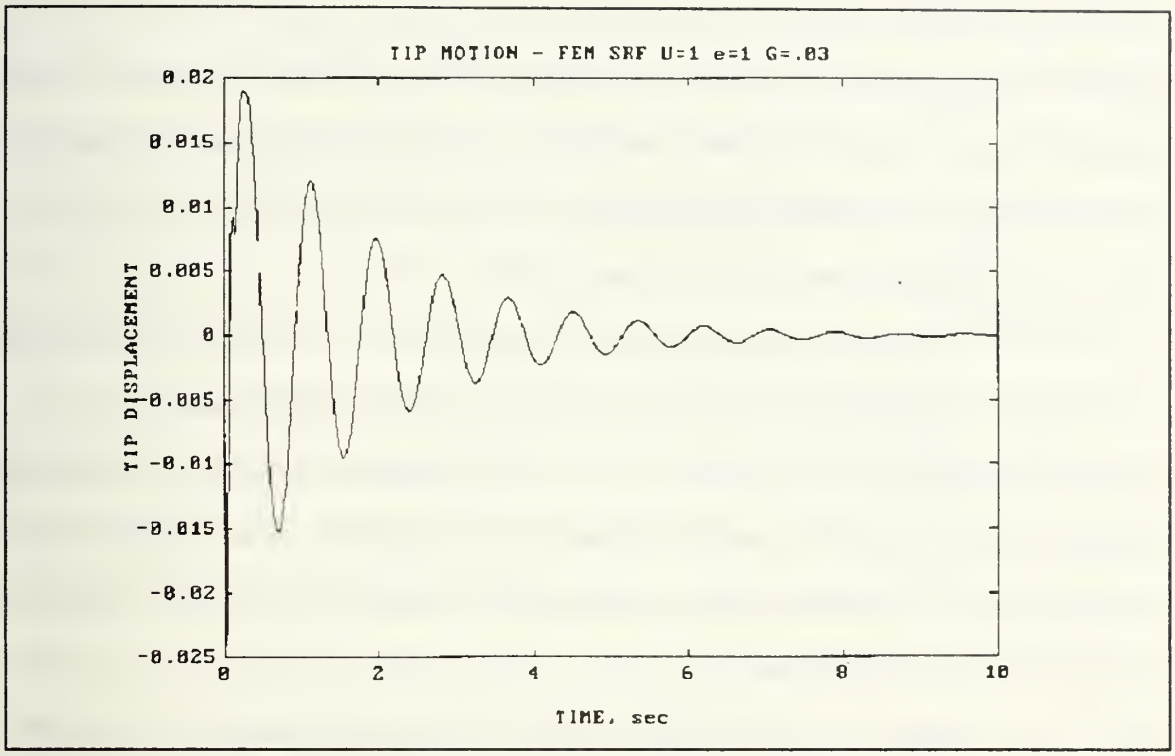

Figure 22 SRF Single Actuator / Negative Gain

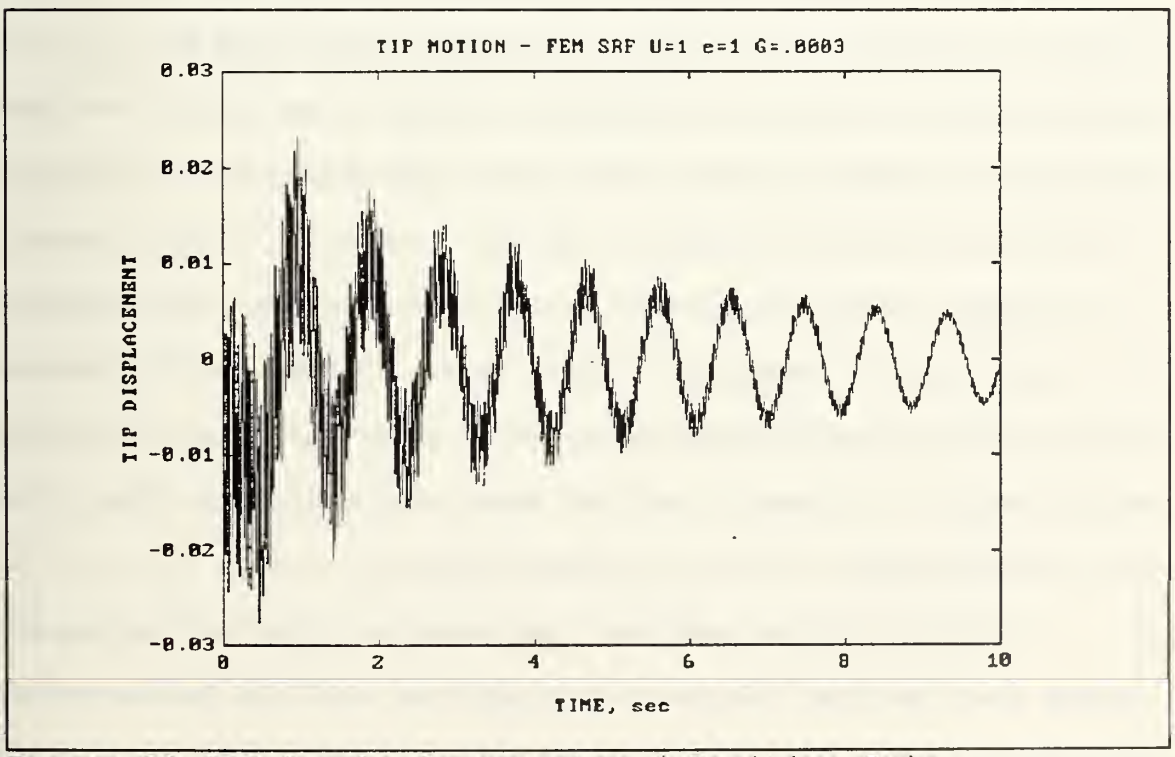

Figure 23 SRF Single Compensator / Positive Gain

form a simple stability condition. The alternate method used was to ensure all the eigenvalues of the system matrix of the state-space equation were negative. Again, two gains were held fixed while varying the third to determine the stable region.

4. Comparison of PPF and SRF

A strict side-by-side comparison of these two methods is not feasible due to the fact that the compensators are not performing the same functions in both methods. Also, since the stable gain regions were so varied, a uniform set of operating parameters that provided sufficient control in both systems could not be defined.

Positive Position Feedback is preferable for applications where a single mode needs to be quickly damped. Control can be maximized by taking advantage of the compensator resonance occurring in the active damping region. PPF also has the advantage of using the sensors to measure the structural displacement rather than the more difficult measurement of structural velocity as is needed with SRF. For multi-modal control, the frequency requirements are too restrictive. One compensator per mode is required in this case. Unless the structural characteristics are uniform and precisely known and unless the compensator is closely matched with the modal frequency, PPF will be operating at less than optimum.

Strain Rate Feedback has the advantage of controlling modes over a wider range of frequencies. As was demonstrated,

a single compensator feeding a single actuator can control three modes. This is important in terms of reducing circuit complexity and manufacture and implementation costs. However, the active damping occurs in a region where the compensator gain is not at a maximum. This has the effect of limiting the amount of control on modes far from the compensator frequency.

The robustness of these two control schemes is demonstrated in Figures 24 and 25. The scenario simulated here is that the actual structural frequencies experienced on-orbit are 10% less than the predicted values around which the compensators were designed. All other parameters are kept constant. This new response of the "modified structure" is shown with the dashed line and is compared to the response of the "original structure" shown with the solid line.

PPF produces almost an identical response for both systems with only miniscule differences. Initial expectations were that this frequency variation would produce a much more significant difference. Further study revealed that the robustness of the system is very dependent on the compensator damping ratio. Small values produce a phase angle curve that approaces a square wave which were seen to emphasize the adverse effects of a frequency change. Likewise, large values stretch out the phase angle curve allowing a less significant change in the system response. For this particular model, the chosen value is large enough to prevent PPF's frequency dependency from degrading the system response. The key to providing

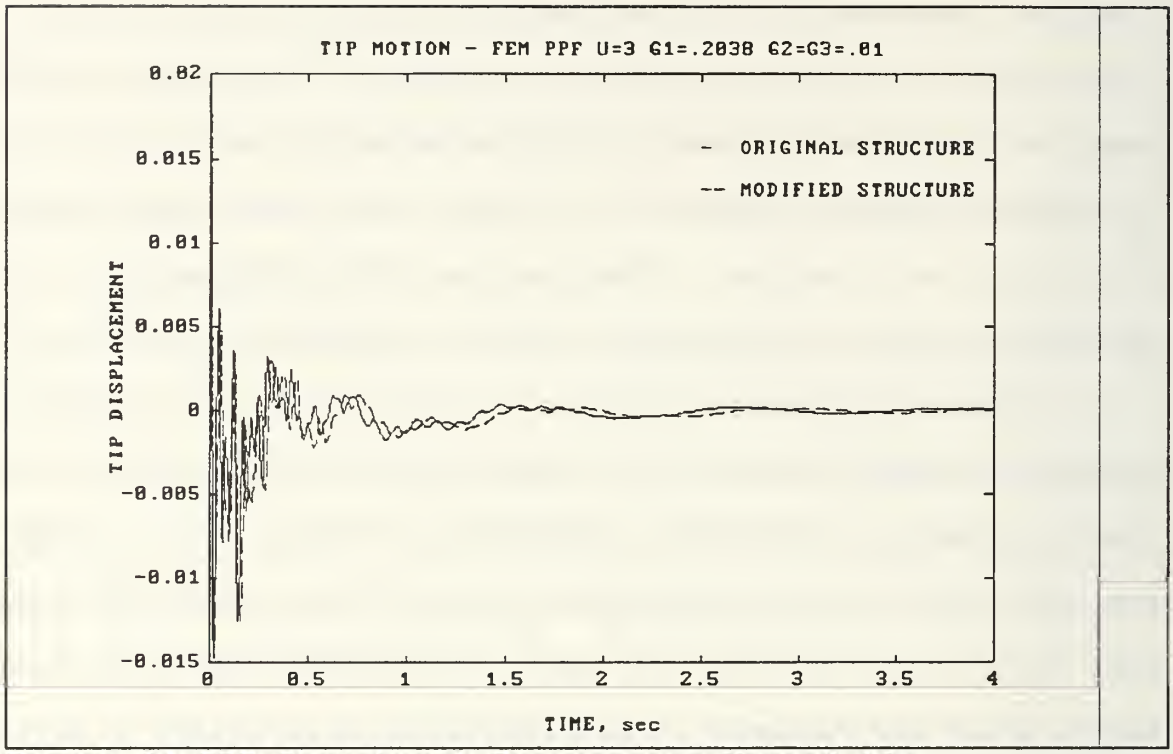

Figure 24 PPF Structural Frequencies Varied 10%

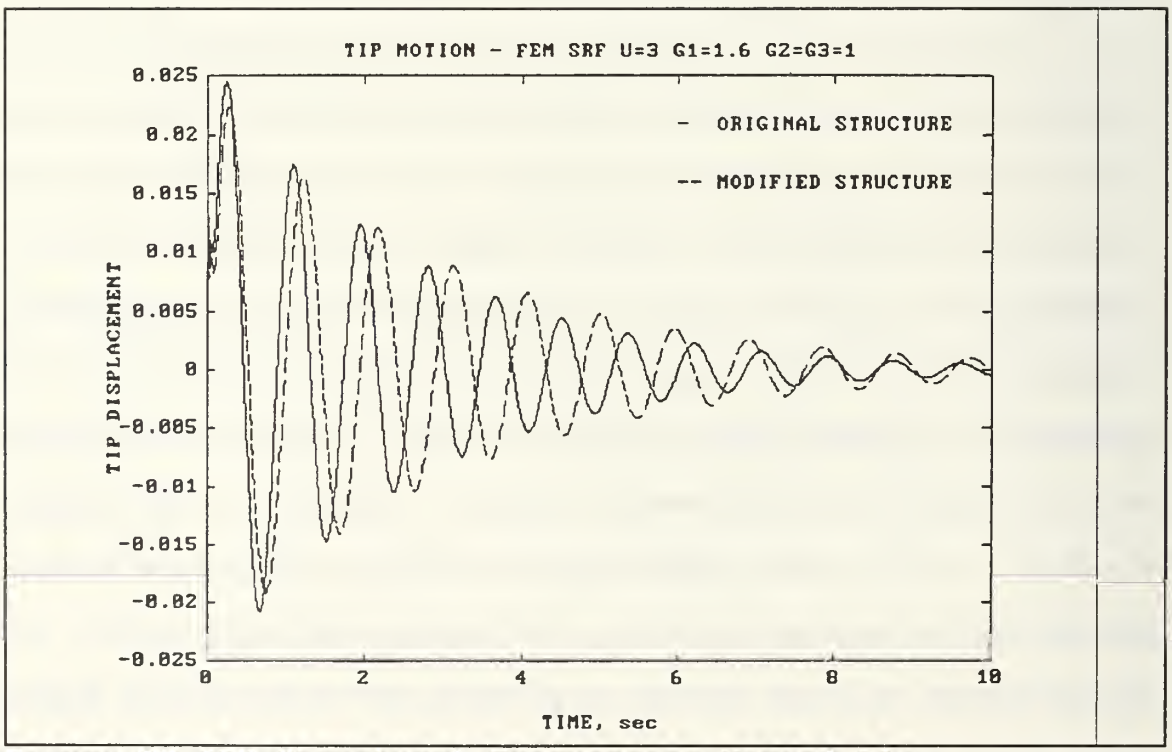

Figure 25 SRF Structural Frequencies Varied 10%

sufficient robustness is to have a moderate compensator damping ratio. Small values will limit the bandwidth of the compensator and large values, while still being robust, will decrease the magnitude of the damping provided.

A variation of only the first mode is seen when using SRF. The "modified" first modal frequency has moved closer to the edge of the bandwidth of the compensators such that the amount of damping able to be provided has decreased slightly. The structure is also more flexible as seen in the lower frequency. SRF is much less dependent on the compensator damping ratio in terms of robustness. The system is operating in a region where the slope of the phase angle curve is not significantly altered by variations of the damping ratio. Simulations showed that the system was equally robust with damping ratios different by two orders of magnitude.

III. EXPERIMENTAL ANALYSIS

The characteristics of Positive Position Feedback will be studied using the Naval Postgraduate School's Flexible Spacecraft Simulator (FSS).

A. PHYSICAL SET-UP

The mechanical lay-out of the experiment is shown in Figure 26. Reference 4 details the circuit design and the choice and placement of the piezoceramic sensors and actuators which comprise the active damping control system. A detailed view of the sensor and actuator locations is shown in Figure 27. The ceramics are mounted on both sides of the flexible arm with opposite polarities such that the sensor voltages and actuator strains are consistent. The damping circuit consists of three sections: a charge amplifier, a low-pass filter and a power amplifier. The components of the filter were chosen such that the compensator values are ω_c = .15 Hz and ζ_c = .1.

For this analysis, the main body of the simulator is held fixed and the flexible arm is the only component affected by external forces. The flexible arm is supported by air pads which allow two-dimensional motion in an approximately frictionless environment.

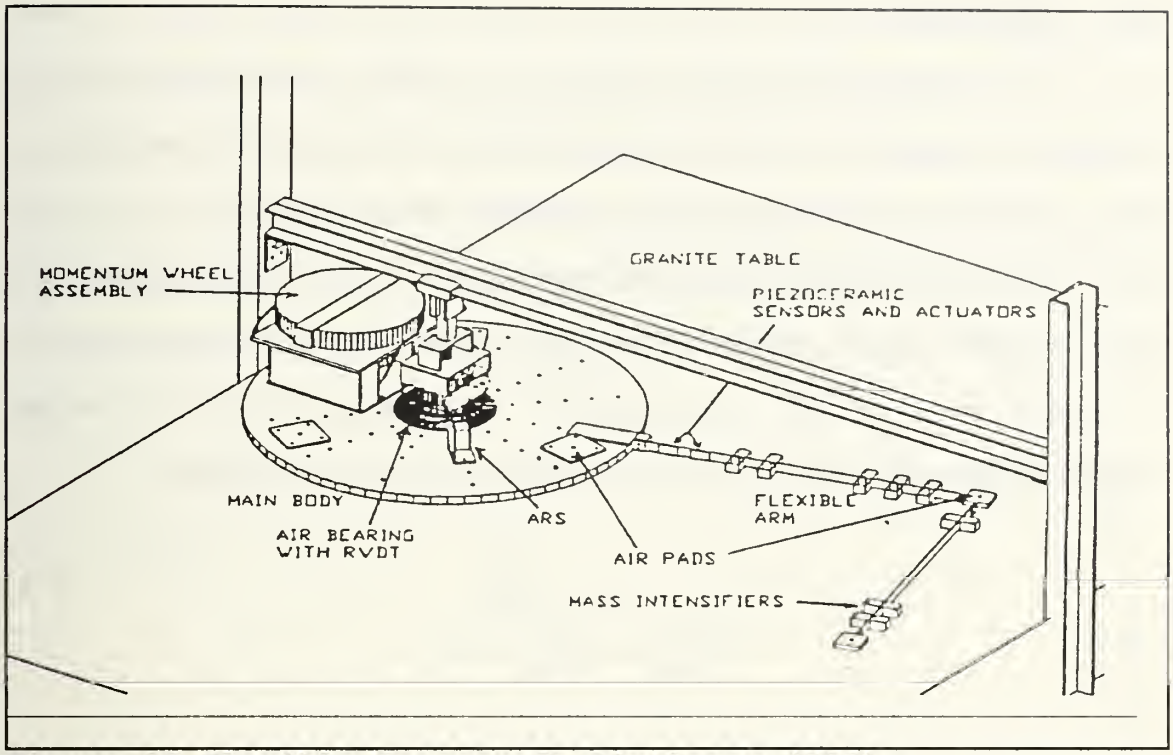

Figure 26 Flexible Spacecraft Simulator (FSS)

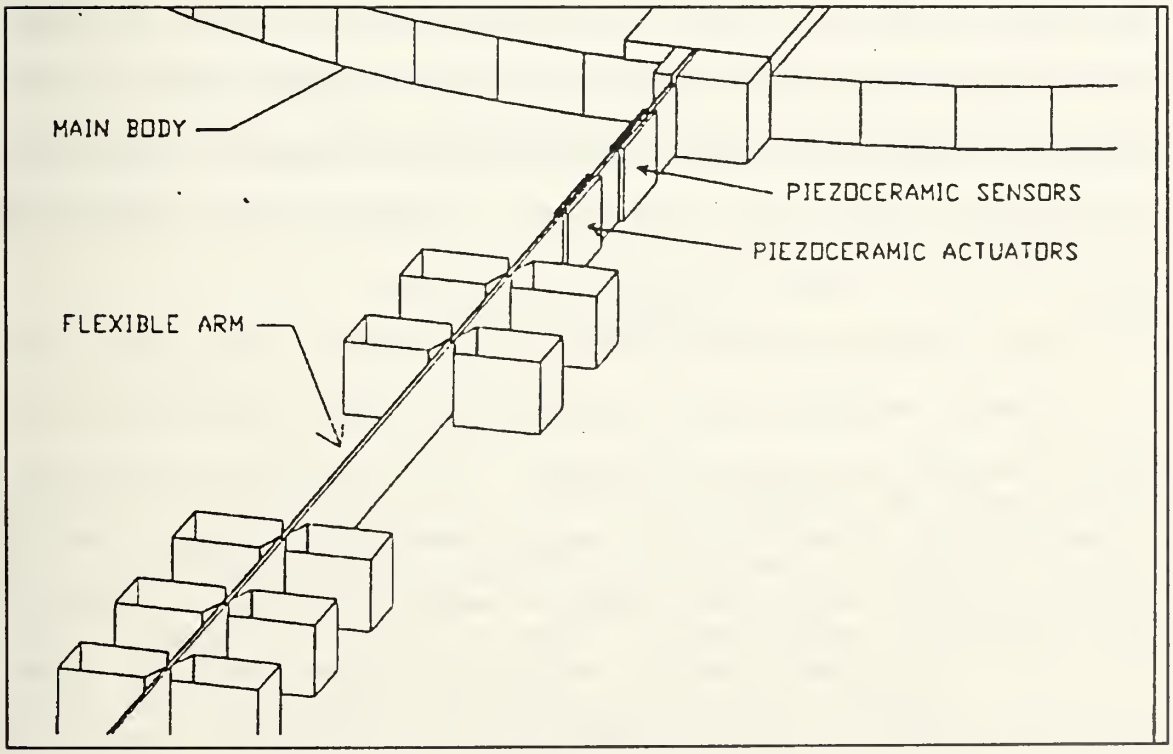

Figure 27 Piezoceramic Locations

B. PROCEDURE

The objective of the experiment was to investigate the effectiveness of the PPF algorithm over a range of structural frequencies and compare the results with theory.

To achieve a variety of frequencies, the configuration of the flexible arm was changed by attaching and detaching the concentrated masses. The natural frequency, ω, for a simple spring-mass system is defined by the relationship:

$$\omega = \sqrt{\frac{k}{m}} \tag{61}$$

where **m** is the mass and **k** is the stiffness. The masses are attached to the arm such that the stiffness remains constant. Therefore, adding mass will lower the frequency from the initial value and vice versa. The selection of where to make mass adjustments was a trial and error procedure until frequencies of sufficient range and separation were found.

Data was obtained in the following manner. The signal from the sensors was sent via a Gould 5900 Signal Conditioner to a Gould RS3800 Stripchart Recorder. This allowed obtaining a time history of sufficient length needed to calculate damping ratios. Phase angle measurements were made using a Hewlett-Packard 54601A Oscilloscope which displayed both the signal from the sensors and the signal to the actuators. Frequency

measurements were made using both sets of equipment. The data was averaged over several run for each configuration.

With only a single compensator in the feedback circuit, the system will only be effective on the mode for which it is designed. Therefore, in this experiment, only the first mode of the flexible arm was excited so that the cleanest and smoothest signal could be recorded.

The damping ratio, ζ, was calculated using the log decrement method:

$$\zeta = \frac{1}{2\pi n} \ln\left(\frac{A_i}{A_f}\right) \tag{62}$$

where A_i is the initial amplitude, A_f is the final amplitude and n is the number of cycles between those two amplitudes. The natural frequency is computed using the damping ratio and the damped period, τ_d:

$$\omega_n = \frac{2\pi}{\tau_d \sqrt{1 - \zeta^2}} \tag{63}$$

However, the damping ratios are small enough with respect to the frequency measurement accuracy that we can assume the natural frequency to be the same as the damped frequency. The phase angle was calculated from the relationship:

$$\phi = \omega \, \Delta t \; (360^\circ/cycle) \tag{64}$$

where ω is the structural frequency in Hz and Δt is the time difference between the sensor and actuator signals as seen on the oscilloscope. The theoretical value for the phase angle at each structural frequency is calculated using Equation 42.

C. RESULTS

As shown in the plot in Figure 28, data was obtained in all three regions of active flexibility, damping and stiffness. (Refer to Figure 9). Although the experimental values

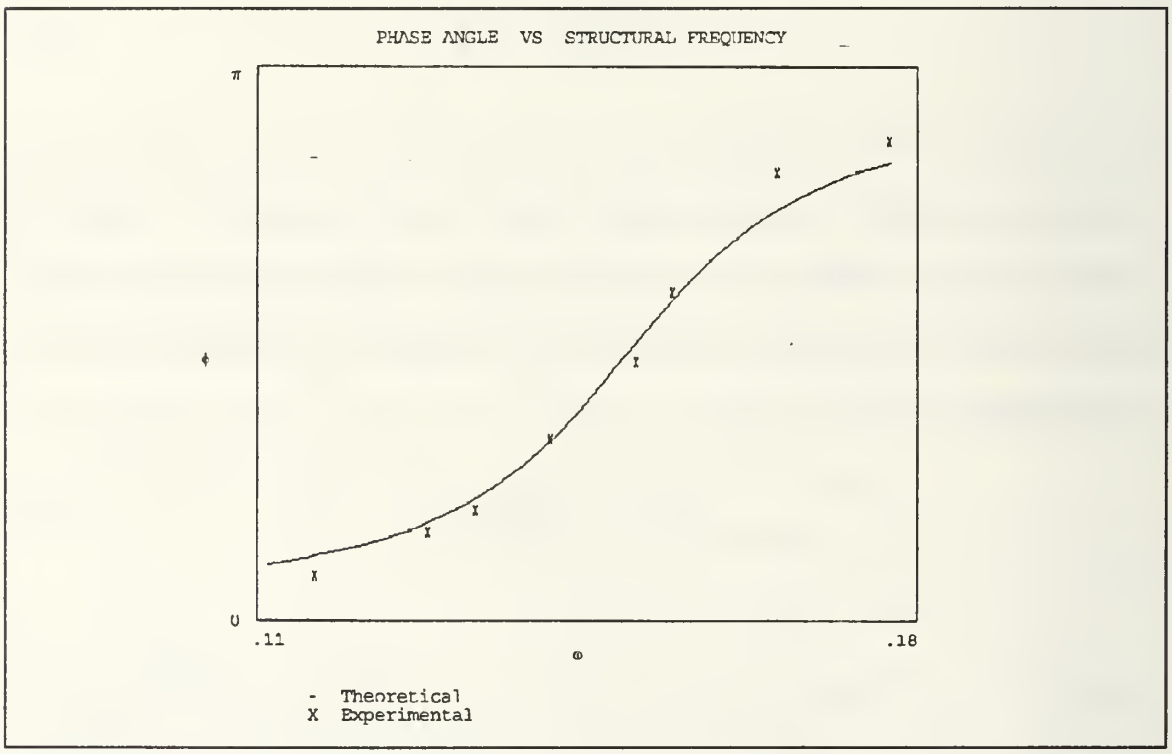

Figure 28 FSS Flexible Arm Phase Angles

for phase angle vary from theory (see Table I) as much as seven degrees in the worst case and considering the +/- 2

degree measurement accuracy, the data clearly follows the trend we expect and we can assume the circuit is functioning properly.

Table I

FLEXIBLE SPACECRAFT SIMULATOR - PPF		
CASE	PHASE ANGLE (Degrees)	
	Theoretical	Experimental
1	19	15
2	29	29
3	32	36
4	55	59
5	90	84
6	111	107
7	139	146
8	150	156

The parameters describing the dynamic response of the flexible arm are listed in Table II. Examining the change in frequency from the freely vibrating (open-loop) to the actively damped (closed-loop) cases, the expected effect on the stiffness term is evident. At the lower frequencies, a decrease is observed indicating the arm has become more flexible. At and near the compensator frequency, there is little or no change. The higher frequencies exhibit an increase meaning the arm has become stiffer.

Table II

FLEXIBLE SPACECRAFT SIMULATOR - PPF					
CASE	FREQUENCY (Hz)		DAMPING RATIO		
	Free	Damped	Free	Damped	% Δ
1	.116	.113	.0095	.0070	-27
2	.128	.125	.0104	.0114	10
3	.133	.128	.0077	.0243	215
4	.141	.140	.0059	.0325	450
5	.150	.150	.0059	.0221	345
6	.154	.156	.0040	.0158	299
7	.165	.168	.0059	.0145	161
8	.177	.180	.0035	.0093	165

A very pronounced variation is seen in the change in the damping ratio when the feedback system is activated. At the lowest observed frequency, the arm has become so flexible that the damping worsens by 27 per cent. There is a steady improvement as the structure moves into the active damping region. The maximum effect is observed with Case 4 showing a 450 per cent improvement. The magnitude of the control provided is best appreciated visually as seen in Figure 29. Even at the higher frequencies, while not in the active damping region, an improvement in the damping ratio is produced by the increased stiffness of the arm.

One discrepancy evident in this data is that the greatest improvement in the damping provided by the compensator does not occur at a structural frequency equal to the compensator frequency. The cause of this variation has been difficult to pin-point. In order for the transfer function resonance peak to occur at .141 Hz, where the maximum increase was observed, the compensator damping ratio would have to increase to .34 or the compensator frequency would have to decrease to .142 Hz. However, this is not consistent with the phase angle data previously mentioned. This rules out any small variations in the feedback circuit as possible sources of error. There are some physical factors which may have caused inconsistencies between the eight configurations. Other experiments were being conducted while this one was in progress which did not allow a uniform orientation of the flexible arm for all of the configurations. Varying frictional or gravitational effects may have adversely affected the consistency of the results. Further detailed experimental work is needed to precisely determine where the maximum effect actually occurs.

This data highlights the advantages and disadvantages of the Positive Position Feedback algorithm. When the compensator is precisely tuned to the structural frequency, the system is operating near the maximum gain of the compensator transfer function. This enables the active damping control to have its greatest effect. However, any deviation from this optimum region reduces the impact of the control system. As seen in this

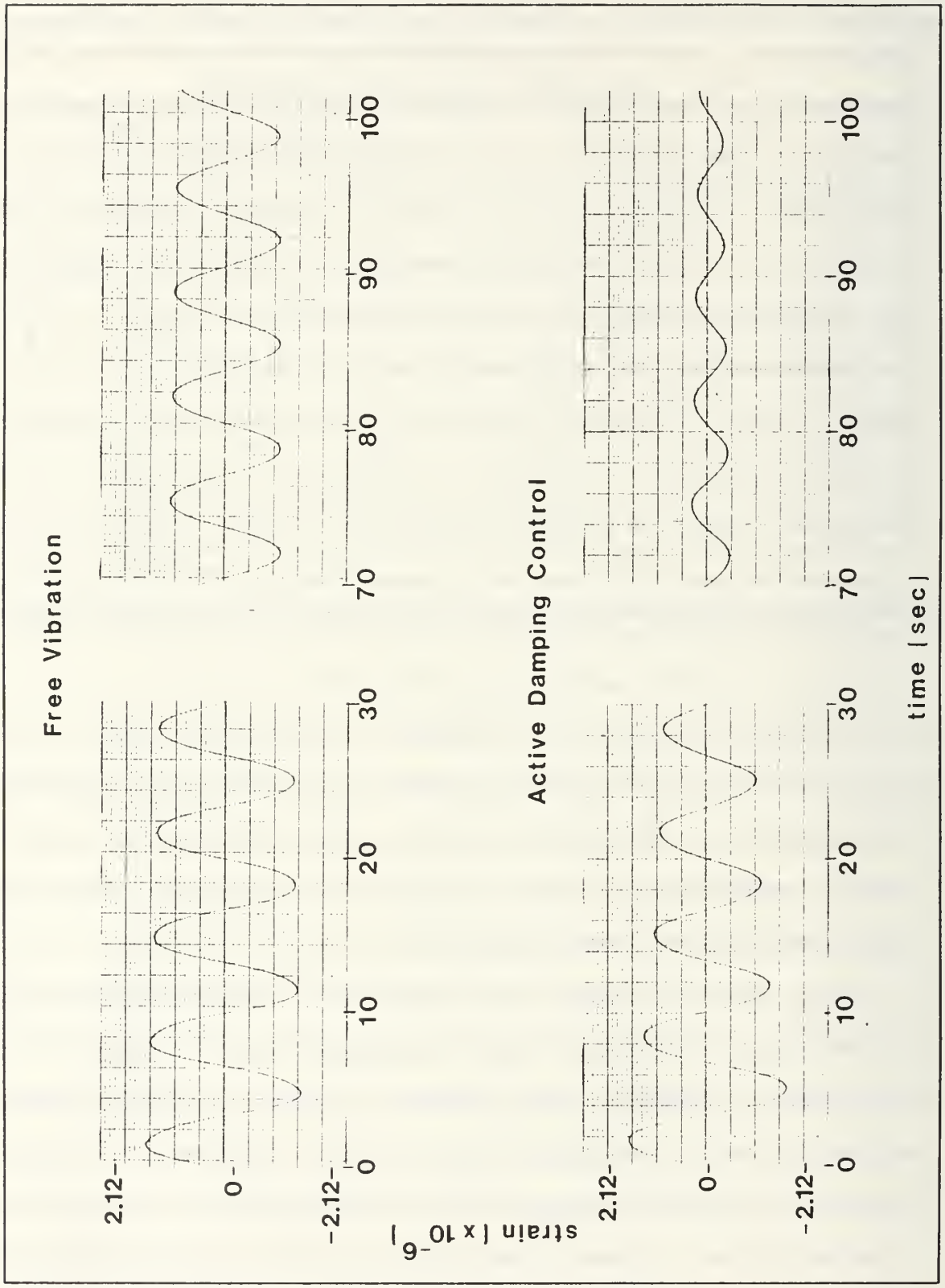

Figure 29 Flexible Arm First Mode Response

experiment, only a 25 per cent reduction in the structural frequency results in the compensator degrading the dynamic response of the system. If the frequencies can not be matched precisely, it is better to err into the active stiffness region where the structural characteristics are not adversely affected. The efficiency of the control law with a bounded gain space, $0<G<1$, is heavily dependent upon the compensator parameters ω_c and ζ_c. It is recommended that moderately higher compensator damping ratios be used so that a relatively large amount of damping is provided while still maintaining sufficient robustness.

IV. CONCLUSIONS

Piezoceramic sensors and actuators have been shown to provide an effective means of controlling structural vibrations. An increase of 450 per cent in the damping ratio of the flexible arm of the Flexible Spacecraft Simulator was demonstrated using the Positive Position Feedback algorithm. This system provides the greatest degree of control when the compensator is precisely tuned to the modal frequency. Its main limitation is that only a single mode can be controlled per compensator.

Positive Position Feedback and Strain Rate Feedback have significantly different control characteristics which were analytically demonstrated for a cantilevered beam. SRF is more advantageous than PPF in the multi-modal environment. With a wider active damping region, it has the ability to stabilize more than one mode given a sufficient bandwidth.

Recommendations for further study include a number of topics. First, the dynamic response of the FSS flexible arm could be improved by incorporating additional compensators into the current configuration. The first mode is very rarely the only mode excited during slew maneuvers and the higher modes should be considered. This problem may be more easily solved by building a Strain Rate Feedback circuit and integrating it with the sensors and actuators currently mounted on the arm. Also, the effect of multiple sensors and actuators on

the arm can be investigated with an optimization study of sensor/actuator placement. There are a variety of control laws which can be used in this application. As an example, a combination of PPF and SRF could be developed which may incorporate the strengths of each and cancel out the weaknesses.

The Flexible Spacecraft Simulator is an excellent tool for studying, not only active damping control techniques, but other spacecraft attitude control and dynamics problems. Current research endeavors include designing an improved thruster for attitude control and incorporating a robotic arm onto the main body.

APPENDIX

```
% Simulation of Beam Vibration using Finite Element Method
% Transformation into modal form using PPF with three control
laws
% utilizing three actuators on elements 1,5,8.
%
% Define physical constants:
%
n=8;                % number of elements
h=.1;               % element length
d=.5;               % element density
EI=.9;                % modulus of elasticity times moment of
inertia
%
% Element mass matrix:
%
Mul=(d*h/420)*[156 22*h; 22*h 4*h^2];
Mur=(d*h/420)*[54 -13*h; 13*h -3*h^2];
Mll=Mur';
Mlr=(d*h/420)*[156 -22*h; -22*h 4*h^2];
%
% Element stiffness matrix:
%
Kul=(EI/h^3)*[12 6*h; 6*h 4*h^2];
Kur=(EI/h^3)*[-12 6*h; -6*h 2*h^2];
Kll=Kur';
Klr=(EI/h^3)*[12 -6*h; -6*h 4*h^2];
%
% Combine matrices for n element system. Disregard first two
rows
% and columns for clamped end.
%
for i=1:n-1,
    M(2*i-1:2*i,2*i-1:2*i)=Mul+Mlr;
    K(2*i-1:2*i,2*i-1:2*i)=Kul+Klr;
%
    M(2*i-1:2*i,2*i+1:2*i+2)=Mur;
    K(2*i-1:2*i,2*i+1:2*i+2)=Kur;
%
    M(2*i+1:2*i+2,2*i-1:2*i)=Mll;
    K(2*i+1:2*i+2,2*i-1:2*i)=Kll;
end
%
M(2*n-1:2*n,2*n-1:2*n)=Mlr;
K(2*n-1:2*n,2*n-1:2*n)=Klr;
%
Mi=inv(M);          % Inverse of mass matrix.
```

```
%
% Obtain eigenvalues and eigenvectors:
%
[phi,lambda]=eig(K,M);
%
% Extract natural freqencies:
%
w=diag(lambda);
%
% Sort from low to high frequency:
%
[w1,num]=sort(w);
w=w(num);
for j=1:2*n
    lambda(j,j)=w(j);
end
%
% Sort eigenvectors:
%
phi=phi(:,num);
%
% Calculate generalized masses:
%
Mg=phi'*M*phi;
%
% Calculate weighted modal matrix:
%
for i=1:2*n
    phiw(:,i)=phi(:,i)/sqrt(Mg(i,i));
end
Mw=phiw'*M*phiw;
Kw=phiw'*K*phiw;
%
% Actuator location matrix (actuators on elements 1,5,8):
%
F=zeros(16,3);
F(2,1)=1;F(8,2)=-1;F(10,2)=1;F(14,3)=-1;F(16,3)=1;
Ft=phiw'*F;
%
% Assign structural modal damping values:
%
z(1)=.0001;z(2)=.0004;z(3)=.0009;z(4)=.0015;z(5)=.0037;z(6)=
.0089;
z(7)=.01;z(8)=.025;z(9)=.042;z(10)=.067;z(11)=.098;z(12)=.11;
z(13)=.35;z(14)=.86;z(15)=1.21;z(16)=1.77;
%
% Assemble structural damping matrix:
%
D=zeros(2*n);
for i=1:2*n
    D(i,i)=2*z(i)*sqrt(Kw(i,i));
```

```
end
%
% Truncate to first three modes:
%
Kw1=Kw(1:3,1:3);
Ft1=Ft(1:3,1:3);
D1=D(1:3,1:3);
%
% Assign compensator values:
%
wc1=sqrt(Kw1(1,1));wc2=sqrt(Kw1(2,2));wc3=sqrt(Kw1(3,3));
zc1=.1;zc2=.1;zc3=.1;
G1=.2038;G2=.01;G3=.01;
Kc=[wc1^2 0 0; 0 wc2^2 0; 0 0 wc3^2];
Dc=[2*zc1*wc1 0 0; 0 2*zc2*wc2 0; 0 0 2*zc3*wc3];
G=[G1 0 0; 0 G2 0; 0 0 G3];
%
% Combine structure and compensator equations into matrix
form:
%
Ds=[D1 zeros(3); zeros(3) Dc];
Ks=[Kw1 -Ft1*G*Kw1; -Kc*Ft1' Kc];
%
% Put closed-loop system in state space form:
%
A=[zeros(6) eye(6); -Ks -Ds];
B=zeros(12,1);
C=eye(12);
D=zeros(12,1);
T=(0:.01:9.99);
U=zeros(T);
X0=zeros(2*n,1);
%
% Initial displacements to excite 3 modes
%
X0(1,1)=.008;X0(2,1)=.05;X0(3,1)=.01;X0(4,1)=0;X0(5,1)=.004;
X0(6,1)=-.086;X0(7,1)=-.007;X0(8,1)=-.086;X0(9,1)=-.016;X0(1
0,1)=0;
X0(11,1)=-.015;X0(12,1)=.01;X0(13,1)=-.001;X0(14,1)=.173;
X0(15,1)=.02;X0(16,1)=.173;
Z0=inv(phiw)*X0;          % Initial displacement in modal
coordinates
Z01=Z0(1:3);
M0=[Z01' 0 0 0 0 0 0 0 0 0]';
[Y,X]=lsim(A,B,C,D,U,T,M0);
%
% Put open-loop system in state-space form:
%
Aol=[zeros(3) eye(3); -Kw1 -D1];
Bol=zeros(6,1);
Col=eye(6);
```

```
Dol=zeros(6,1);
M0ol=[Z01' 0 0 0];
[Yol,Xol]=lsim(Aol,Bol,Col,Dol,U,T,M0ol);
%
%
% Convert back to tip physical coordinate:
%
phiq=phiw(1:16,1:3);
for i=1:1000
    tm=[Y(i,1) Y(i,2) Y(i,3)]';
    q=phiq*tm;
    tip(i)=q(15);
    tmol=[Yol(i,1) Yol(i,2) Yol(i,3)]';
    qol=phiq*tmol;
    tipol(i)=qol(15);
end
%
% Plot data
%
plot (T,tip(:))
xlabel ('TIME, sec')
ylabel ('TIP DISPLACEMENT')
title ('TIP MOTION - FEM PPF U=3 G1=.2038 G2=G3=.01')
pause
plot (T,tipol(:))
xlabel ('TIME, sec')
ylabel ('TIP DISPLACEMENT')
title ('TIP MOTION - FEM OPEN LOOP')
pause
```

REFERENCES

1. Betros, Robert S., and Bronowicki, Allen J., "Seminar Notes," *Active Damping Workshop*, Spring, 1991.

2. Chen, J.C., and Fanson, J.L., "Structural Control by the Use of Piezoelectric Active Members," *Proceedings of NASA/DOD CSI Technology Conference* held in Norfolk, VA 18-21 November 1986, pp. 809-829.

3. *Guide to Modern Piezoelectric Ceramics*, pp. 4-5, Vernitron Corporation, Bedford, OH.

4. Jones, Evan S., *Development of an Active Damping System to Aid in the Attitude Control of Flexible Spacecraft*, pp. 16-25, Master's Thesis, Naval Postgraduate School, Monterey, CA, December 1991.

5. Hanagud, S., Obal, M.W., and Calise, A.J., "Optimal Vibration Control by the Use of Piezoceramic Sensors and Actuators," *Journal of Guidance, Control and Dynamics*, v. 15, no. 5, pp. 1199-1206, September-October, 1992.

6. Craig, Roy R. Jr., *Structural Dynamics: An Introduction to Computer Methods*, p.386, John Wiley & Sons, Inc., 1981.

7. Junkins, John L., and Kim, Youdan, *An Introduction to Dynamics and Control of Flexible Structures*, pp. 73-74, to be published in American Institute of Aeronautics and Astronautics Education Series, 1992.

8. Fanson, J.L., and Caughey, T.K., "Positive Position Feedback Control for Large Space Structures," *American Insitute of Aeronautics and Astronautics Journal*, v.28, no. 4, pp. 717-724, April, 1990.

BIBLIOGRAPHY

Agrawal, B.N., Bang, H., and Hailey, J., "Application of Piezoelectric Actuators and Sensors in the Vibration Control of Flexible Spacecraft Structures," IAF-92-0319, World Space Congress, Washington, D.C., 28 August - 5 September 1992.

Aubrun, J.N., "Theory of the Control of Structures by Low-Authority Controllers," *Journal of Guidance and Control*, v.3, no. 5, pp. 444-451, 1980.

Bailey, T., and Hubbard, J.E. Jr., "Distributed Piezoelectric-Polymer Active Vibration Control of a Cantilever Beam," *Journal of Guidance and Control*, v. 8, no. 5, pp. 605-611, 1985.

Bathe, Klaus-Jurgen, *Finite Element Procedures in Engineering Analysis*, Prentice Hall, Inc., NJ, 1982.

Bayo, Eduardo, "A Finite-Element Approach to Control the End-Point Motion of a Single-Link Flexible Robot," *Journal of Robotic Systems*, v. 4, no. 1, pp. 64-75, 1987.

Cavin, R.K. III, and Dusto, A.R., "Hamilton's Principle: Finite-Element Methods and Flexible Body Dynamics," *American Institute of Aeronautics and Astronautics Journal*, v.15, no. 12, pp. 1684-1690, December 1977.

Gerhold, Carl H., and Rocha, Rodney, "Active Control of Flexural Vibrations in Beams," *Engineering, Construction and Operations in Space, Proceedings of Space 88*, pp. 482-494 American Society of Civil Engineers, 1988.

Goh, C.J., and Caughey, T.K., "On the Stability Problem caused by Finite Actuator Dynamics in the Collocated Control of Large Space Structures," *Int. Journal of Control*, v. 41, no.3, pp. 787-802, 1985.

Kagawa, Y., and Gladwell, G.M.L., "Finite Element Analysis of Flexure-Type Vibrators with Electrostrictive Transducers," *IEEE Transactions on Sonics and Ultrasonics*, v. SU-17, no. 1, pp. 41-49, 1970.

Kim, Youdan, Junkins, John L., and Kurdilla, Andrew J., "On the Consequences of Certain Modeling Approximations in Dynamics and Control of Flexible Space Structures,"

Meirovitch, L., *Computational Methods in Structural Dynamics*, Sitjhoff and Noordhoff, 1980.

Reddy, J.N., *An Introduction to the Finite Element Method*, McGraw Hill Book Co., NY, 1984.

Reddy, J.N., *Applied Functional Analysis and Variational Methods in Engineering*, McGraw Hill Book Co., NY, 1986.

Schaechter, David B., "Optimal Local Control of Flexible Structures," *Journal of Guidance and Control*, v. 4, no. 1, pp. 22-26, 1979.

Thomson, William T., *Theory of Vibration with Applications*, Prentice Hall, NJ, 1988.

INITIAL DISTRIBUTION LIST

1.	Defense Technical Information Center Cameron Station Alexandria, VA 22304-6145	2
2.	Library, Code 52 Naval Postgraduate School Monterey, CA 93943-5002	2
3.	Chairman, Code AA Department of Aeronautics and Astronautics Naval Postgraduate School Monterey, CA 93943	1
4.	Chairman, Code SP Department of Aeronautics and Astronautics Naval Postgraduate School Monterey, CA 93943	1
5.	Professor Brij N. Agrawal, Code AA/Ag Department of Aeronautics and Astronautics Naval Postgraduate School Monterey, CA 94943	2
6.	Professor Hyochoong Bang, Code AA/Ba Department of Aeronautics and Astronautics Naval Postgraduate School Monterey, CA 94943	1
7.	LT Scott M. Newman, USN 4328-102 Bedrock Circle Baltimore, MD 21236	1